ENEA

Agenzia nazionale per le nuove tecnologie,
l'energia e lo sviluppo economico sostenibile

Ricerca di Sistema elettrico

Analisi del comportamento del combustibile MOX ad elevato burnup in condizioni di normal operation e DBA

D. Rozzia, N. Forgione, A. Ardizzone, A. Del Nevo

ANALISI DEL COMPORTAMENTO DEL COMBUSTIBILE MOX AD ELEVATO BURNUP IN CONDIZIONI DI NORMAL OPERATION E DBA

D. Rozzia, N. Forgione (UNIPI), A. Ardizzone (POLITO), A. Del Nevo (ENEA)

Settembre 2013

Titolo

Analisi del comportamento del combustibile MOX ad elevato burnup in condizioni di normal operation e DBA

Descrittori

   Tipologia del documento: **Rapporto Tecnico**
   Collocazione contrattuale: Accordo di programma ENEA-MSE su sicurezza nucleare e
                                reattori di IV generazione

   Argomenti trattati: Sicurezza nucleare
                                Generation IV reactors
                                Combustibile nucleare

Sommario

Il documento costituisce il contributo alla task A.3 dell'Accordo Di Programma 2012. L'obiettivo dell'attività è l'analisi delle capacità del codice TRANSURANUS versione 2012 nel predire il comportamento del combustibile tipo MOX sviluppato appositamente per reattori tipo "Fast Breeder (a sodio)" in condizioni di tipo DBA (Design Basis Accident). Particolare enfasi è data alle principali variabili che influenzano la simulazione del profilo di temperature nel combustibile ed I fenomeni ad esso connessi durante le escursioni di potenza fino al principio di fusione sulla base dell'esperimento HEDL-P-19. Detto test è stato condotto nel reattore veloce EBR-II (USA) al fine di investigare l'effetto della larghezza del gap iniziale tra pellets e camicia, da 0.086 a 0.25 mm, sulla potenza lineare richiesta per causare principio di fusione al centro di un combustibile MOX a inizio vita. Il database include 16 FBR barrette MOX fresche incamiciate con camicia in acciaio INOX tipo 316 (lavorato a freddo al 20%).
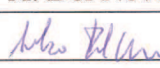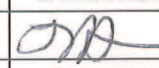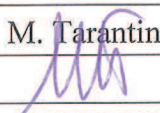
ENEΛ

Note

* Autori:
D. Rozzia (UNIPI), N. Forgione (UNIPI), A. Ardizzone (POLITO), A. Del Nevo (ENEA)

Copia n.			In carico a:				
1			**NOME**				
			FIRMA				
0	**EMISSIONE**	**18/09/13**	**NOME**	A. Del Nevo *	I. Di Piazza	M. Tarantino	
			FIRMA				
REV.	**DESCRIZIONE**	**DATA**		**REDAZIONE**	**CONVALIDA**	**APPROVAZIONE**	

(This page has been intentionally left blank)

Abstract

The capability of the fuel to operate at high power without melting is of interest to FR's because reactor design limits normally require that there be a low probability of fuel melting during steady-state operation including overpower conditions. This requirement has a direct effect on the steady-state power limit of the fuel pin and the reactor. Optimization of this power capability is important to reactor thermal efficiency and economy of operation. Due to the high temperature drop achieved in the pellet to cladding gap at beginning of life, it is necessary to check the power needed to cause fuel melting at reactor start-up even for fuels designed to operate at high burn-ups.

The HEDL-P-19 experiment was conducted during 1971 in the EBR-II reactor to investigate the effects of initial fuel-to-cladding diametric gap sizes, from 0.086 to 0.25 mm, on the linear-heat-rate needed to cause incipient fuel melting at beginning-of-life. The test included 16 FBR fresh MOX fuel rods clad with cold worked type 316 stainless.

The present document constitutes the contribution LP2.a.3_c to the task A.3 of ADP-2012. The aim of the activity is to summarize the main results obtained after the simulations of 16 FBR fuel rods included in the above mentioned database by means of TRANSURANUS code. Particular emphasis is given to the main variables which influence the prediction of the fuel temperature profile and its related phenomena during power excursion. The activity is based on the comparison between experimental data collected at the end of the test and simulated trends (i.e. axial extent of melting, columnar grain radius, central void formation, gap size). The importance of the sensitivity analysis, as tool to address the relevance selected parameters and code models on the results is also discussed.

This document consists of four main sections and two attached appendixes. Section one points out the objective and the framework of the activity. The HEDL-P-19 experiment is described in section two. The section includes the procedure adopted to develop the TRANSURANUS reference input decks. Sections three constitutes the core of this report. It aims to investigate the capabilities of TRANSURANUS code in simulating HEDL-P-19 experiment. This is pursued by systematic comparison between simulated and measured trends and by extensive comparative analyses among selected models. Conclusions are finally given in section four. Appendix A and B report detailed figures in support to the comparative analyses.

CONTENTS

Abbreviations

ADS	Accelerator Driven System
ADP	Accordo Di Programma
ALFRED	Advanced Lead cooled Fast Reactor
ASTRID	Advanced Sodium Test Reactor for Industrial Demostration
BOL	Beginning Of Life
CIRTEN	Consorzio Interuniversitario per la Ricerca Tecnologica Nucleare
CW	Cold Worked
DIMNP	Dipartimento di Ingegneria Meccanica Nucleare e della Produzione
EBR-II	Experimental Breeder Reactor #2
ENEA	Agenzia nazionale per le nuove tecnologie, l'energia e lo sviluppo economico sostenibile
FBR	Fast Breeder Reactor
FP	Fission Product
FR	Fast Reactor
FRAPCON-3	"Steady state fuel rod performance code"
GEN-IV	GENeration - IV
He	Helium
HEDL	Hanford Engineering Development Laboratory
ITU	Institute for Transuranium Elements
LFR	Lead cooled Fast Reactor
LHR	Linear Heat Rate
LWR	Light Water Reactor
MA	Minor Actinide
MHYRRA	Multi-purpose HYbrid Research Reactor
MOX	Mixed OXide (fuel)
NPP	Nuclear Power Plant
OD	Outer Diameter
O/M	Oxygen to Metal ratio
PIE	Post Irradiation Examination
Pu	Plutonium
PWR	Pressurized Water Reactor
SFR	Sodium cooled Fast Reactor
RTL	Ramp Terminal Level
RR	Ramp Rate
SS	Stainless Steel
TD	Theoretical Density
TU	TRANSURANUS
U	Uranium
UNIPI	Università di Pisa
UO_2	Uranium Oxide

List of figures

List of tables

1 Introduction

1.1 Background

Wherever uranium fuels are used as a source of power, the management, use and disposal of plutonium and plutonium containing fuel and wastes are intrinsic aspects of the technology. The reactor recycle strategy identifies three main temporal phases[1][2][3].

- The first phase has seen a gradual introduction of the recycling of mixed oxide fuel up to an industrial scale in light water reactors in several countries, is currently well established. MOX usage in LWRs is a well understood and mature technology and MOX can be managed in a very similar way to uranium fuel. The current inventory of separated civil plutonium is safely stored and has still to be recycled. The necessary safeguards arrangements have kept pace with these developments wherever plutonium is handled, fabricated, stored, transported and irradiated.

- The second phase (up to, say, 2030) is beginning at the time of writing. It is characterized by an ongoing but irregular expansion of MOX recycling in which new countries will acquire MOX technology and additional nuclear plants will be licensed for MOX fuel. It could then be expected that the stockpiles of separated plutonium (both civil and weapons surplus) will begin to diminish and move to significantly lower levels during this phase. As well as extending the number of power plants loading MOX fuel, the technology now needs to be developed for advanced reactors such as the GEN-IV Fast Reactors (i.e. LFR or SFR) or Accelerator Driven Systems (i.e. MHYRRA). Additionally, more environmentally friendly reprocessing methods with reduced emissions will be needed to prepare for the third and long term phase of plutonium recycle and management.

- In this preparation for the third phase of development, emphasis must be placed on both achieving greater public acceptance for plutonium fuel technology as well as making the power producing utilities more attractive economically. These same utilities will be the ultimate source of the financing needed to establish the stable development of nuclear power based on uranium and, over the longer term, plutonium fuels. A fuel that is more expensive than others or which may limit reactor operation is unacceptable for the power producers. If the economic and performance targets cannot be reached and negative public attitudes persist, there will be no third phase of plutonium recycle. However, if such a development can be realized, the third phase should see the progressive introduction of advanced thermal reactors as well as fast reactors, alongside new technologies specifically designed for MOX fuel. The aim will be to manage the production and use of plutonium effectively to avoid major stockpiling.

In thermal reactors, it is generally accepted that MOX fuel behaves similar to UOx fuel and should therefore wind stand the same safety requirements. Compared to UOx, MOX fuel mainly differentiates by: lower conductivity, lower melting point, higher creep rate, higher FGR, lower gaseous swelling and production / release of He coming from alpha decay of heavy Minor Actinides[1][2]. In general, these differences depend on the fabrication process and upon the PuO_2 content. Since the experimental databases on MOX fuel are not so extended as for UOx, there is a growing interest in understanding the MOX fuel behavior both for the application in commercial LWR fuels with high burn-ups performance and next generation FRs. In particular, the characterization of MOX fuel for FR application is of great importance to develop advanced fuel design since FR MOX fuel has unique features: it contains larger quantities of PuO_2 than LWR, it is operated at higher temperature and in harder neutron energy spectrum environment.

1.2 Objective of the activity

The capability of the fuel to operate at high power without melting is of interest to FR's because reactor design limits normally require that there be a low probability of fuel melting during steady-state operation including overpower conditions. This requirement has a direct effect on the steady-state power limit of the fuel pin and the reactor.

In particular, due to the high temperature drop achieved in the pellet to cladding gap at beginning of life (BOL), it is necessary to check the power needed to cause fresh fuel melting even for fuels designed to operate at high burn-ups.

The aim of this report is the assessment of TRANSURANUS[4][5][6] code version 2012 in simulating FR-MOX fuel behavior with particular reference to inception of fuel melting during reactor start-up. To fulfill the objective, HEDL P-19[7][8] test has been reconstructed and modeled by means of TU code. The test was conducted in EBR-II during 1971 and investigated the melting propensity of sixteen 25% PuO_2 enriched fresh fuel whose design was typical of the Fast Flux Test Facility (FFTF).

2 Description of the experiment and development of the input decks

2.1 The HEDL-P-19 Experiment

The HEDL P-19[7][8] test was designed to provide "integral" power-to-melt data on 25% PuO$_2$ enriched fuel. The fuel pin fabrication parameters simulate the FFTF/FBR design conditions[9]. The test was irradiated in row 2, position 2B1 in the EBR-II during reactor run 48E[10]. The positions immediately adjacent to the test were occupied by EBR-II driver fuel assemblies. HEDL P-19 aimed to investigate the effects of initial fuel-to-cladding gap sizes, from 0.043 to 0.127 mm, on the linear-heat-rate needed to cause incipient fuel melting at beginning-of-life.

P-19 was an encapsulated 19-pin subassembly, it consisted of 8 fresh pins with cladding outside diameters 5.84 mm, and 8 fresh 6.35 mm OD pins. The fresh pins were clad with 316 stainless steel (20% cold worked). All pins were backfilled with pure helium during fabrication. The experiment consisted of:

- Slow power increase up to selected conditioning level held for 1 hr
- Rapid power increase up to a designed power level held for 10 minutes
- Reactor scram

The summary of the design parameters and operating conditions is included in Tab. 1. The EBR-II power history during HEDL-P-19 is given in *Fig. 1*. *Fig. 2* reports the axial power profile of the pins.
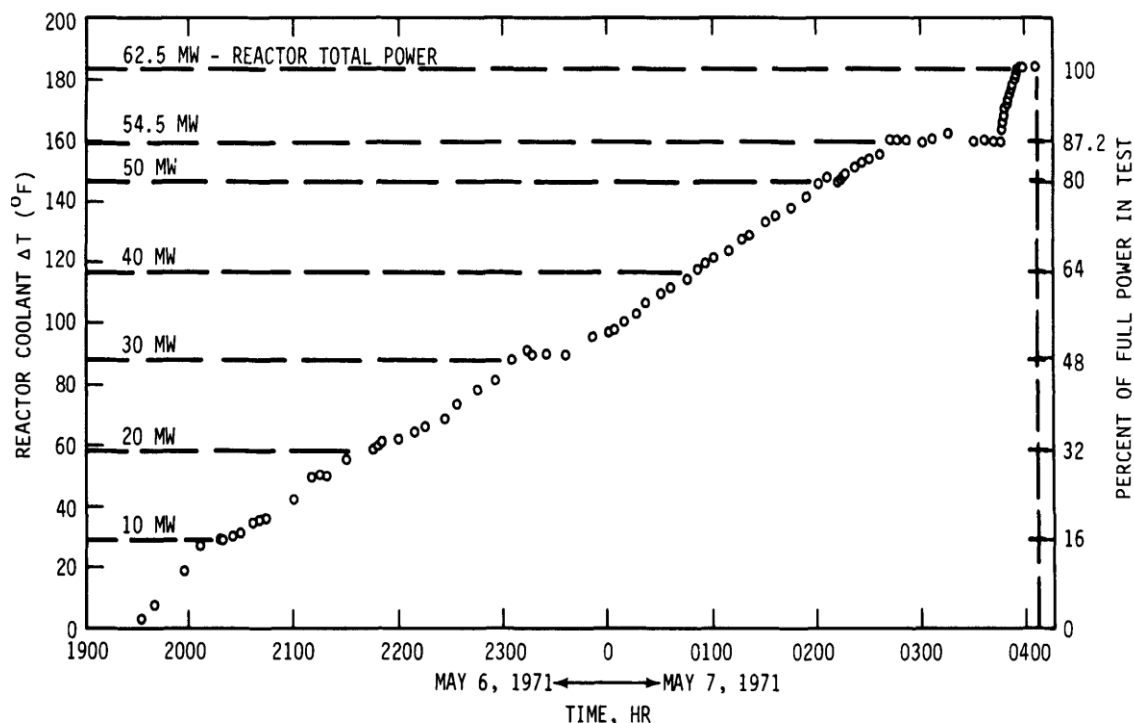

Fig. 1 – EBR-II power history.
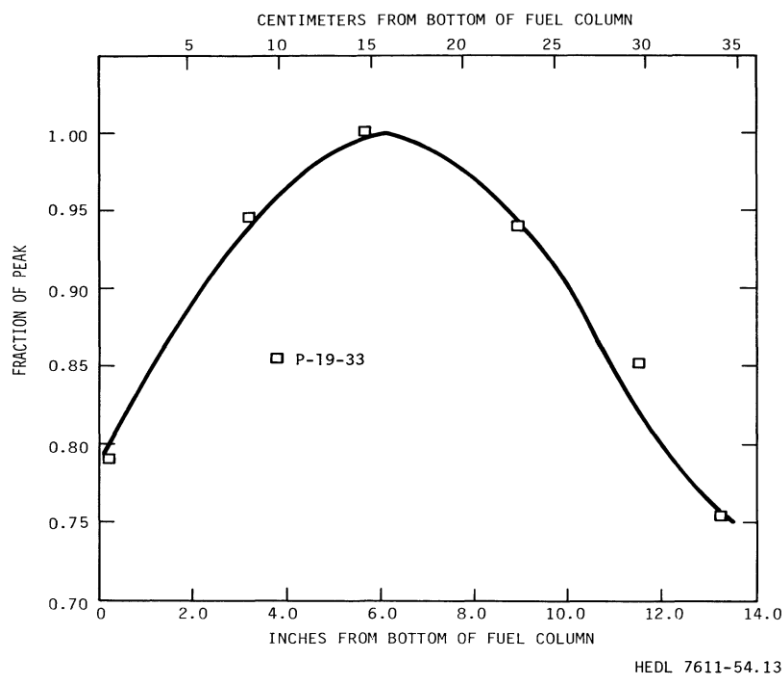
Fig. 2 – HEDL P-19, pin power axial profile.

Rod N°		1	2	3	4	5	6	7	8	9	10	11	12	13	14	15	16
Rod Id.		P 19 2	P 19 3R	P 19 5	P 19 6	P 19 7R	P 19 8	P 19 13	P 19 20	P 19 24R	P 19 25R	P 19 26R	P 19 27R	P 19 28	P 19 30	P 19 33	P 19 35
Gap μm		99	127	72.5	49.5	79	122	99	123	127	101.5	76	51	43	89	62.5	91.5
%TD	90.75	X		X	X		X	X	X							X	X
	92.40		X			X				X	X	X	X	X	X		
Clad OD mm	5.84	X		X	X		X	X	X							X	X
	6.35		X			X				X	X	X	X	X	X		
Fuel		— 25% PUO₂ - 75% UO₂
Cladding		316 stainless steel (20% cold worked)
Filling gas		98% He at 1 bar
O/M		1.96
Active length		343 mm
Na inlet temp.		371 ℃
Max LHR kW/m		54.5	64	56.1	56.1	66.6	53.8	54.5	54.1	64.6	66	66.9	66.9	67.9	65.6	55.1	54.1

Tab. 1 – HEDL P-19 design data.

2.1.1 Main achievements from the experiment

After irradiation, the P-19 pins were removed from EBR-II and neutron radio-graphed. This confirmed partial fuel melting in a number of pins. All 5.84 mm OD pins with fuel-to-cladding gaps equal to or less than 0.14 mm had no fuel melting. The remaining 5.84 mm OD pins and all the 6.35 mm OD pins experienced partial fuel melting[7][8].

The capsules were then returned to HEDL where detailed destructive examination was conducted. Transverse fuel ceramographic samples were used to obtain measurements of fuel restructuring zone radii, central void and residual fuel-to-cladding gaps. They were also used to obtain the radial extent of melting at the peak power locations of those pins experiencing partial fuel melting. However, power to-melt data calculated from transversal sections were considered less accurate than those obtained from longitudinal sections because of the uncertain influence of relocated molten fuel on local power. Further, the radial extent of central void formation at these locations is uncertain; melting has obliterated the central void formed by restructuring. Since most of these peak power regions operated at much higher powers than Q'm, melting is extensive even in adjacent fuel. The axial extents of

melting, as determined from longitudinal ceramographic sections, offered the best data for determining Q'm since these sections were actually located where incipient melting occurred and experienced the least power variation due to molten fuel relocation. The main data from PIE are given in Tab. 2, Tab. 3 and Tab. 4.

Rod Id	Peak Power [kW/m]	EXP Bottom axial Melting extent			EXP Top axial Melting extent		
		Location [cm]	Local power [kW/m]	Coolant Temp [°C]	Location [cm]	Local power [kW/m]	Coolant Temp [°C]
P-19-2	54.5	72.1	51.8	386	248.4	50.5	426
P-19-3R	64.0	8.9	52.5	373	312.9	51.5	451
P-19-5	56.1	--	--	--	--	--	--
P-19-6	56.1	--	--	--	--	--	--
P-19-7R	66.6	40.9	59.1	381	286.3	56.8	448
P-19-8	53.8	63.2	50.9	384	266.2	48.6	429
P-19-13	54.5	84.6	52.8	389	339.0	51.5	424
P-19-20	54.1	98.3	52.5	392	270.3	48.6	431
P-19-24R	64.6	15.0	52.8	374	320.0	49.5	453
P-19-25R	66.0	21.1	55.1	376	305.1	52.8	452
P-19-26R	66.9	46.7	60.4	382	281.3	59.7	445
P-19-27R	66.9	59.2	61.7	386	258.6	60.7	442
P-19-28	67.9	59.7	62.0	386	271.8	59.1	446
P-19-30	65.6	28.2	56.4	378	288.3	56.1	448
P-19-33	55.1	--	--	--	--	--	--
P-19-35	54.1	82.8	52.5	388	224.5	52.5	421

Tab. 2 – HEDL P-19, axial extension of fuel melting at the end of the experiment.

Rod Id	EXP Bottom axial Melting extent			EXP Top axial Melting extent		
	Central void radii [mm]	Columnar grain radii [mm]	TD at pellet centre [%]	Central void radii [mm]	Columnar grain radii [mm]	TD at pellet centre [%]
P-19-2	0.38	1.52	98.0	0.36	1.55	96.4
P-19-3R	0.41	1.85	97.2	0.41	1.85	96.9
P-19-7R	0.38	1.55	98.6	0.38	1.73	97.4
P-19-8	0.41	1.58	98.0	0.43	1.60	98.0
P-19-13	0.38	1.52	98.0	0.36	1.55	98.0
P-19-20	0.41	1.58	97.4	0.43	1.58	97.3
P-19-24R	0.20	1.70	92.9	0.20	1.70	93.1
P-19-25R	0.23	1.73	93.6	0.46	1.80	98.5
P-19-26R	0.38	1.52	98.6	0.43	1.68	98.2
P-19-27R	0.31	1.52	96.1	0.36	1.45	98.4
P-19-28	0.23	1.45	94.5	0.20	1.47	94.5
P-19-30	0.33	1.65	96.0	0.38	1.65	97.9
P-19-35	0.38	1.70	96.0	0.41	1.63	96.6

Tab. 3 – HEDL P-19, measurements of central void, columnar grain radius and TD at pellet centre at the end of the experiment.

Rod Id	Id	Location [cm]	Central void radii [mm]	Molten radii [mm]	Columnar grain radii [mm]	Diametric gap [mm]
P-19-2	1	15.5	0.64	0.94	1.80	0.142
	2	19.1	0.58	0.79	1.73	0.142
P-19-5	1	15.5	0.46	0.00	1.68	0.102
	2	18.5	0.48	0.00	1.65	0.147
	3	20.3	0.43	0.00	1.55	0.102
	4	21.6	0.46	0.00	1.60	0.122
P-19-6	1	15.5	0.36	0.00	1.58	0.071
	2	17.8	0.36	0.00	1.50	0.069
	3	18.8	0.38	0.00	1.52	0.091
	4	20.1	0.38	0.00	1.58	0.074
	5	21.3	0.38	0.00	1.40	0.071
	6	22.6	0.33	0.00	1.40	0.084
P-19-8	1	15.5	0.46	0.97	1.85	0.208
P-19-24R	1	15.5	0.18	1.14	2.11	0.107
P-19-25R	1	15.5	0.99	1.21	2.11	0.124
	2	18.5	0.79	0.89	2.03	0.104
P-19-26R	1	15.5	0.64	0.71	1.91	0.102
	2	18.8	0.69	1.19	2.01	0.079
	3	19.8	0.76	0.91	1.93	0.104
	4	20.8	0.13	0.76	1.85	0.091
P-19-27R	1	15.5	0.33	1.02	1.85	0.069
	2	18.5	0.74	0.84	1.88	0.084
	3	20.3	0.51	0.69	1.85	0.071
	4	20.8	0.00	0.91	1.85	0.064
	5	21.8	0.56	0.74	1.78	0.094
P-19-28	1	15.5	0.00	0.86	1.80	0.086
	2	18.5	0.00	0.97	1.85	0.066
	3	20.3	0.69	0.91	1.85	0.064
	4	20.8	0.56	0.71	1.80	0.071
	5	21.8	0.23	0.86	1.85	0.051
P-19-30	1	15.5	0.99	1.32	2.01	0.076
	2	17.5	0.94	1.24	2.06	0.076
	3	19.3	0.18	1.30	2.08	0.074
P-19-33	1	15.5	0.43	0.00	1.63	0.086
	2	17.5	0.43	0.00	1.60	0.127
	3	19.3	0.41	0.00	1.65	0.130
	4	20.8	0.43	0.00	1.60	0.114
	5	22.1	0.36	0.00	1.50	0.112
P-19-35	1	15.5	0.58	0.76	1.75	0.124
	2	19.3	0.00	0.79	1.75	0.165
	3	20.8	0.20	0.81	1.75	0.150

Tab. 4 – HEDL P-19, transversal measurements of central void, molten radius, columnar grain radius and gap size at the end of the experiment.

2.2   Development and setup of the TRANSURANUS models

2.2.1   Description of the HEDL P-19 input deck

The activity is performed using TRANSURANUS code, version "v1m1j12", with the deterministic option, steady state thermal and mechanical analysis[4][5][6]. The version of the manual is "v1m1j12". The boundary conditions are prepared using a program written in PERL language.

Suitable physical models are chosen for the simulation of MOX fuel behavior subjected to power ramp condition. The models selected are generally the ones standard for the transient to be simulated excepts fuel relocation and fuel conductivity that have been subjected to comparative analyses (see section 3). The fuel melting temperature was measured and reported in the database: 2760°C. Accordingly, the standard melting criterion (that depends on PuO_2 content, O/M ratio and burn-up), is deactivated and the exact value is introduced in the source of the code.

Only the active part of the fuel is accounted for the simulation. It has been divided into 17 axial sections that have been obtained from *Fig. 2*. The nominal design values are used if available (see°Tab. 1). The fuel average grain size and the gas plenum length are not reported in the database, they have been assumed, respectively, 22 μm (average grain diameter) and 300mm (close to the active length).

2.2.2   Selection of the boundary conditions

The boundary conditions implemented for the analysis are:

- linear heat rate at 17 axial position,
- sodium bulk temperature histories (same position of linear power),
- heat transfer coefficient at cladding outer surface (two values are given in the database), and
- coolant pressure (0.1 MPa).

The detailed procedure adopted to reconstruct of the power histories is not discussed in this report, for any question on this topic please contact daviderozzia@libero.it. The rate of power increase during the final ramp is not given, it has been fixed at 500 kW/ (m*h), according to typical power ramp tests[11]. The average and axial peak values implemented as boundary conditions for rod P-19-2 are given in *Fig. 3* and *Fig. 4* as sample.
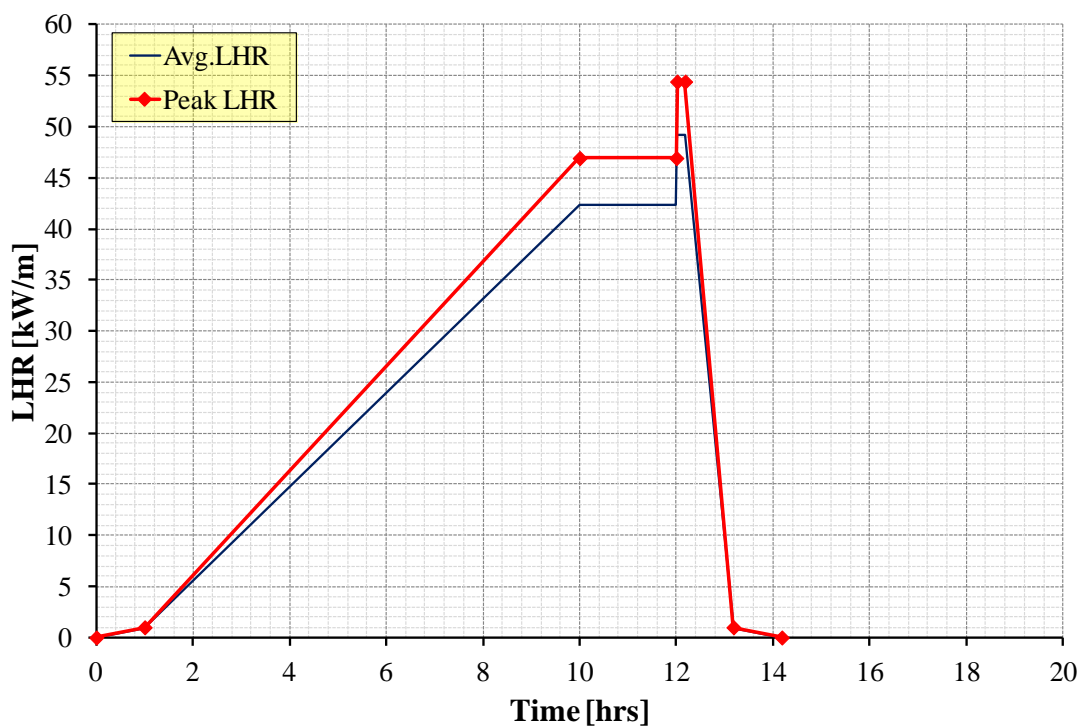
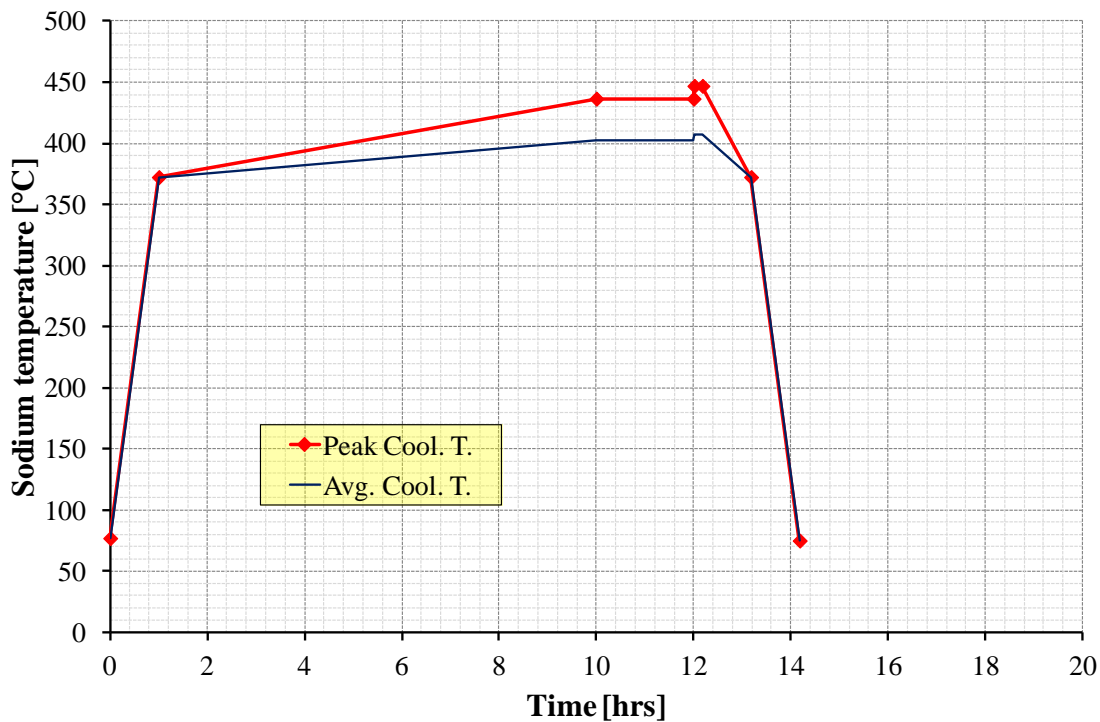*Fig. 3 – HEDL P-19, rod P-19-2 average and peak axial linear power history.*

Fig. 4 – HEDL P-19, rod P-19-2 average and peak axial bulk coolant temperature history.

3 Assessment of TU code against HEDL P-19 experiment

The prediction of the fuel melting at beginning of life mainly depends on the correct simulation of the gap width and on the simulation of the fuel temperature radial profile. This analysis is therefore focused on the assessment of the simulation of the gap size and, once the gap is verified to be captured, on the assessment of the fuel conductivity correlations (that directly impact on the fuel temperature)[12].

3.1 Simulation of the gap size: cracking and relocation effects

In this preliminary analysis, the fuel conductivity has been selected according to the original correlation of Wiesenack[13]. Comparative assessment among the fuel conductivity correlation is presented in section 3.2. The choice of the relocation model mainly influences the gap width during the irradiation. In fact, pellet cracking and relocation promotes the movement of pellet fragments toward the cladding. Five different options are available in the code. They have been described in Ref.∘[14].

- REL0 deactivates the relocation.
- The original KWU-LWR model (REL2) accounts for the as fabricated gap, for tangential and axial relocation and it applies also when gap is closed[6].
- The GAPCON-THERMAL-3 (REL3) accounts for the tangential strain due to relocation depending on the as fabricated gap, the burn-up (exponential function that saturates at 5MWd/kgU), the linear heat rate (a simple function). It does not consider the axial strain and it applies also when gap is closed[6].
- The modified KWU-LWR (REL5) accounts for the tangential and axial strain due to relocation depending only on the as fabricated gap. It applies also when gap is closed[6].
- The modified FRAPCON-3 (REL8) is the standard relocation model. It accounts only for the tangential strain due to relocation depending on the as fabricated gap, the burn-up, the linear heat rate. It does not apply when gap is closed[6]

The gap size is measured at one or more axial elevations at the end of the test, the main results are summarized in Tab. 5 and *Fig. 5*. The table contains the maximum measured and predicted ranges while the figure highlights all the experimental data.

The experimental and predicted gap trends at the end of the test as function of the axial elevation are presented in detail for each rod from *Fig. 6* to *Fig. 11*. Appendix A includes: the gap trend in the peak axial position as function of time (from *Fig. A. 1* to *Fig. A. 8*), and the effect relocation on the axial extension of fuel melting (from *Fig. A. 9* to *Fig. A. 16*). This last datum is not discussed with detail since it is considered in the assessment of fuel conductivity (section 3.2).

Deactivating the relocation model (REL0), due to the densification effects, the gap is overestimated and predicted to increase compared to its initial size (see *Tab. 5* and *Fig. A. 1* as sample). This causes high temperature drop in the gap region and, consequently, increases the melting propensity (see from *Fig. A. 9* to *Fig. A. 16*). Opposite considerations apply to REL2 that tends to under predict the gap width excepts for rods P-19-24R, P-19-25-R and P-19-30, *Fig. 5*. REL3, REL5 and REL8 are, with same exceptions probably connected with relocation of melted fuel, generally in agreement with the experiment being the standard model REL8 those that fits the experimental trend in the best manner. Excepts REL0, gap closure during the test occurs in any simulation of rods P-19-27R and P-19-28

(Fig. A. 6 and *Fig. A. 7)*. REL 2 and REL5 predict further gap closure in rods P-19-6 and P19-26R (*Fig. A. 2* and *Fig. A. 6)*. P-19-7R experiences gap closure in REL2 (*Fig. A. 3)*.

N°	Rod Id	Initial gap [μm]	EXP gap [μm]	REL0 gap [μm]	REL2 gap [μm]]	REL3 gap [μm]	REL5 gap [μm]]	REL8 gap [μm]]
1	P-19-2	99	71	102-104	58-59	75-79	72-74	70-72
3	P-19-5	72.5	51-73	76-77	44-45	56-59	46-48	53-54
4	P-19-6	49.5	34-45	53-55	29-32	41-42	22-26	38-40
6	P-19-8	122	104	126-127	70-71	91-97	89-90	86-88
9	P-19-24R	127	54	130-131	70-72	91-98	91-92	88-90
10	P-19-25R	101.5	52-62	104-105	58-59	74-79	73-74	71-72
11	P-19-26R	76	40-52	79-80	44-46	55-59	48-50	54-55
12	P-19-27R	51	32-47	54-55	30-36	39-43	24-39	38-40
13	P-19-28	43	26-43	46-48	28-38	34-36	21-39	33-37
14	P-19-30	89	37-38	92-93	52-53	64-70	62-63	63-64
15	P-19-33	62.5	43-69	67-68	39-40	50-51	37-38	47-48
16	P-19-35	91.5	62-82	95-97	54-56	70-73	65-67	65-67

Tab. 5 – HEDL P-19, influence of the relocation model on the final gap size, summary of the results.
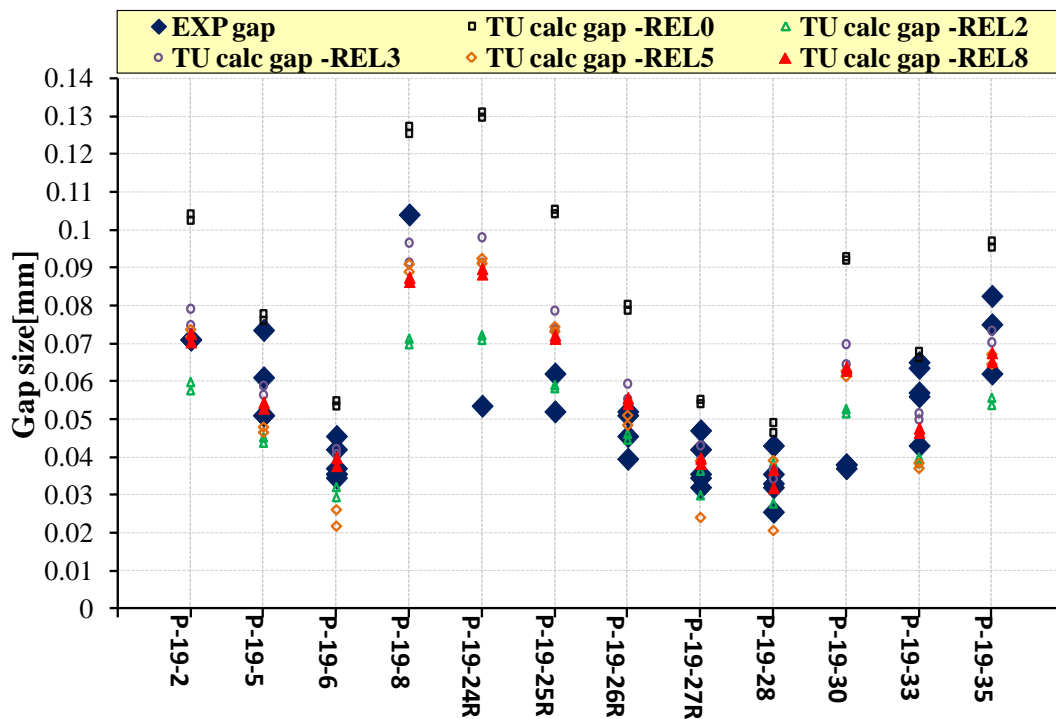
Fig. 5 – HEDL P-19, influence of the relocation model on the final gap size, summary of the results.
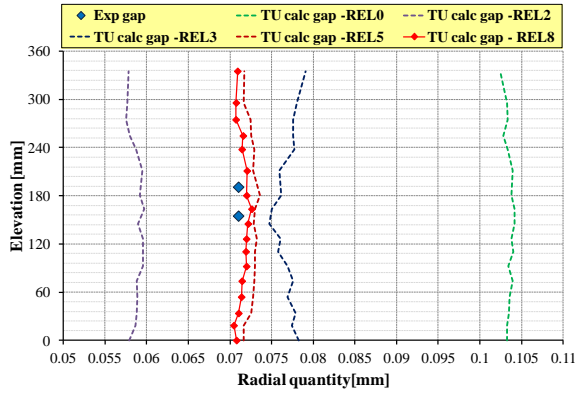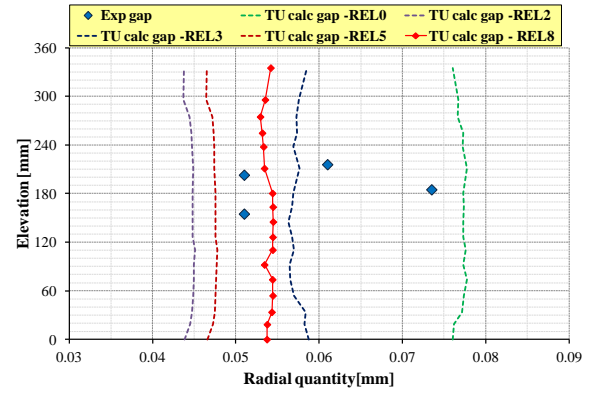
Rod P-19-2   *Rod P-19-5*

Fig. 6 – HEDL P-19, influence of the relocation model on the final gap size, rods #1, 3.
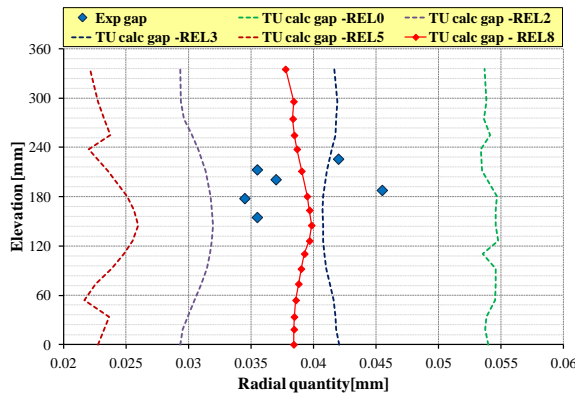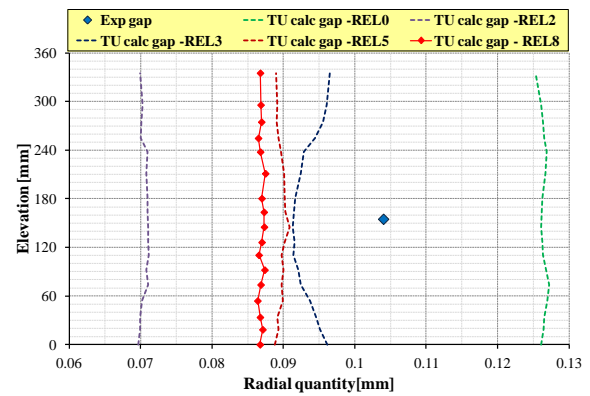
Rod P-19-6   *Rod P-19-8*

Fig. 7 – HEDL P-19, influence of the relocation model on the final gap size, rods #4, 6
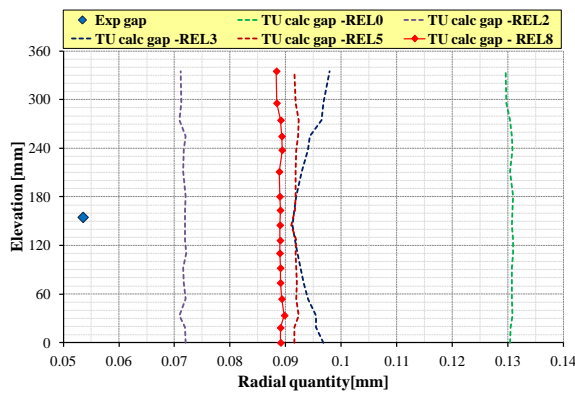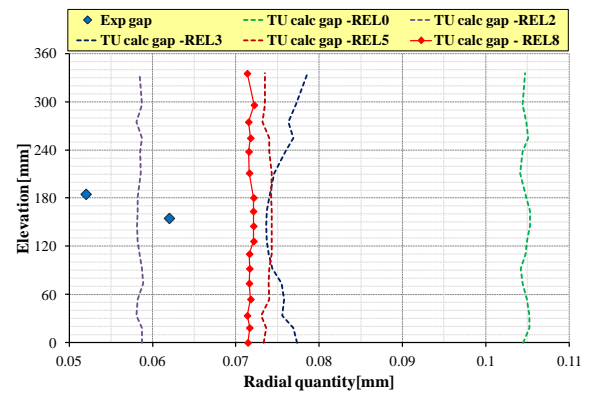
Rod P-19-24R   *Rod P-19-25R*

Fig. 8 – HEDL P-19, influence of the relocation model on the final gap size, rods #9, 10
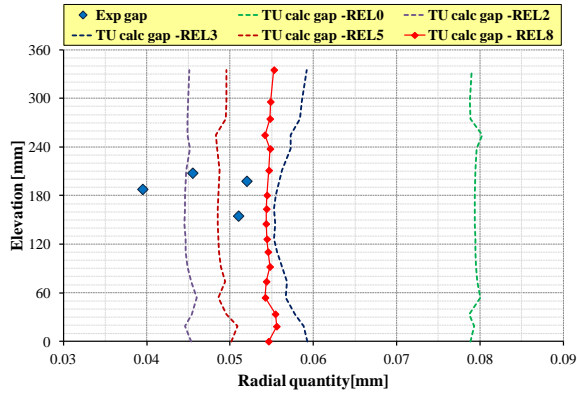
Rod P-19-26R
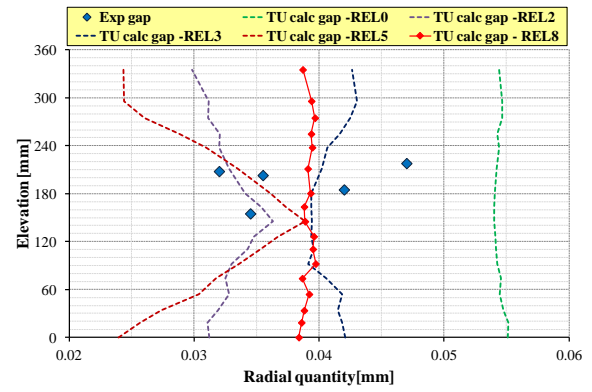
Rod P-19-27R

Fig. 9 – HEDL P-19, influence of the relocation model on the final gap size, rods #11, 12
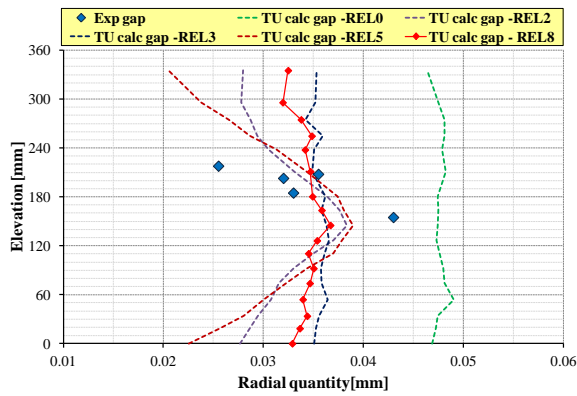
Rod P-19-28
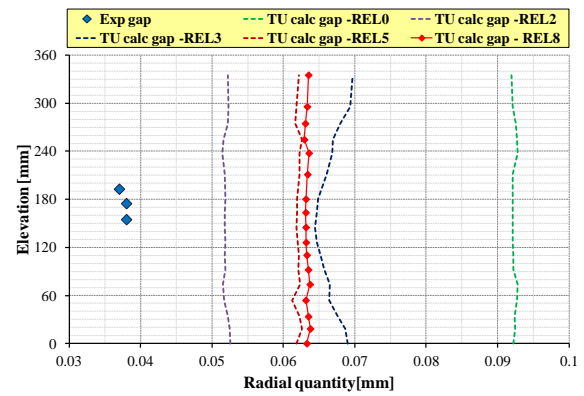
Rod P-19-30

Fig. 10 – HEDL P-19, influence of the relocation model on the final gap size, rods #13, 14
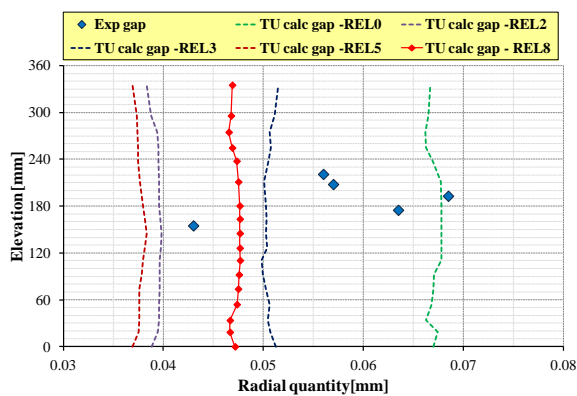
Rod P-19-33
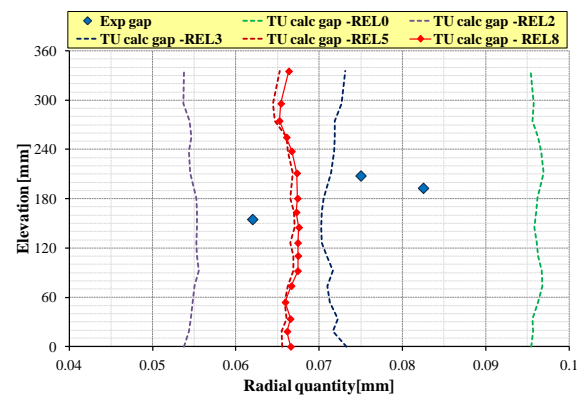
Rod P-19-35

Fig. 11 – HEDL P-19, influence of the relocation model on the final gap size, rods #15, 16

3.2 Simulation of fuel temperature profile: fuel conductivity effects

This analysis is conducted assuming the standard relocation model, REL8. Five different correlations are available in the code to treat MOX conductivity. They have been described in Ref.∘[14].

- CND1 is according to the correlation of Philipponneau[15]. It accounts for the local temperature, the local burn-up, the local porosity and O/M.
- CND31 is the TU standard MOX correlation fitted to ITU data[16]. It accounts for the influence of the local temperature, the local burn-up, and the local porosity.
- CND32 is the original MOX correlation of Carbajo et al[17]. It accounts for the local temperature, the local burn-up, the local porosity, the O/M, the dissolved and precipitated FPs and the radiation effects.
- CND33 is the original MOX correlation of Lanning and Beyer[18]. It accounts for the local temperature, the local burn-up, the local porosity and the O/M.
- CND34 is the original correlation of Wiesenack[13]. It is derived from the UO_2 correlation reduced by a constant factor of 0.92.

It should be mentioned that, even if these correlations are recommended for both LWR and FBR MOX, they have been mainly tested on LWR MOX fuel which is operated at lower temperature and contains less PuO_2 than FBR fuel. Therefore, discrepancies are expected and may be related to uncertainty of the correlations in the high temperature zone (particularly beyond 2200°C that is always exceeded in the experiment) or to the effect of the high PuO_2 content (which is not directly considered in any correlation).

The main results are summarized in Tab. 6. The axial extension of melting is analyzed for each rod from *Fig. 12* to *Fig. 19*. The time dependent fuel centreline temperature and the fraction of molten fuel in the peak axial section is reported for the first six rods in detail in Appendix B from *Fig. B. 1* to *Fig. B. 12*. The influence of the conductivity correlations on the final gap size is depicted in Appendix B from *Fig. B. 13* to *Fig. B. 17*.

Rod P-19-2 and rod P-19-6 are analyzed in *Fig. 12, Fig. 13*, and *Fig. B. 1, Fig. B. 2, Fig. B. 7, Fig. B. 8 Fig. B. 13* and *Fig. B. 14* as samples. The first rod had a fabricated gap of 99μm a pellet density of 90.75%TD and a cladding outer diameter of 5.84mm (see Tab. 1). It was ramped up to 54.5 kW/m and experienced melting at its radial centre for about 180mm along its axial elevation, *Fig. 12*. The correlations provide different extensions of the axial melting front. In particular, CND1, CND31, CND32 and CND33 over predict this phenomenon being CND33 more close to the experiment. CND34 (that has been obtained from a correlation developed for UO_2) under-predicts the axial melting front. These considerations generally apply to the rods that experience fuel melting in the experiment, Tab. 6.

Rod P-19-6 had a fabricated gap of 49.5μm a pellet density of 90.75%TD and a cladding outer diameter of 5.84mm (see Tab. 1). It was ramped up to 56.1 kW/m and did not experience melting, *Fig. 13*. Only correlation CND34 agrees with the experiment while the remaining correlation are conservative and predict fuel melting. Again, these considerations can be extended to the rods that did not melt in the experiment (P-19-5, P-19-6, P19-33), Tab. 6.

The conductivity correlation has a minor influence on the gap size at the end of the test, see Appendix B from *Fig. B. 13* to *Fig. B. 17* (this justify the independent assessment of the relocation models).
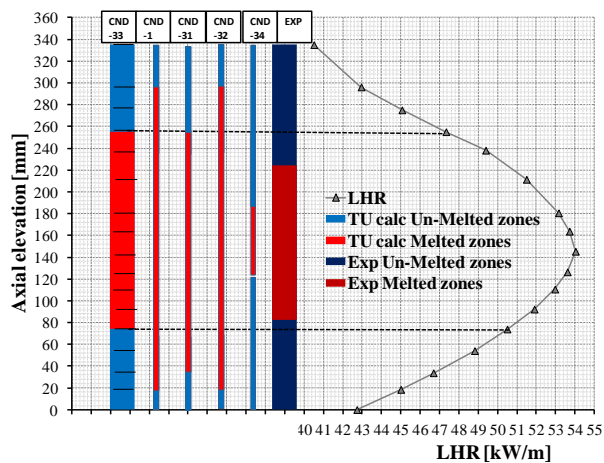
The fuel centreline temperature in peak axial position may exceed 3500°C depending on the correlation adopted being their difference up to few hundreds °C. Consistently, the fraction of molten fuel in the peak axial section may overpass 30% (see Appendix B from *Fig. B. 1* to *Fig. B. 12*).

Rod Id	EXP melting extent [mm]	CND1 melting extent [mm]	CND31 melting extent [mm]	CND32 melting extent [mm]	CND33 melting extent [mm]	CND34 melting extent [mm]
P-19-2	72.1-248.4	0.0-296.0	33.8-275.1	0.0-296.0	54.1-255.1	110.6-211.4
P-19-3R	8.9-312.9	0.0-343.0	0.0-343.0	0.0-343.0	0.0-343.0	18.5-296.2
P-19-5	--	18.5-296.2	54.1-255.1	18.5-296.2	54.1-255.1	126.4-145.3
P-19-6	--	33.8-275.1	92.3-211.4	54.1-255.1	92.3-211.4	--
P-19-7R	40.9-286.3	0.0-343.0	0.0-343.0	0.0-343.0	0.0-296.0	54.1-255.1
P-19-8	63.2-266.2	0.0-343.0	18.5-296.2	0.0-343.0	33.8-275.1	73.9-238.1
P-19-13	84.6-239.0	0.0-296.0	33.8-275.1	0.0-296.0	54.1-255.1	111.6-211.4
P-19-20	98.3-270.3	0.0-343.0	18.5-296.2	0.0-343.0	18.5-275.1	73.9-238.1
P-19-24R	15.0-320.0	0.0-343.0	0.0-343.0	0.0-343.0	0.0-343.0	18.5-296.2
P-19-25R	21.1-305.1	0.0-343.0	0.0-343.0	0.0-343.0	0.0-343.0	33.8-275.1
P-19-26R	46.7-281.3	0.0-343.0	18.5-296.2	0.0-343.0	18.5-296.2	54.1-255.1
P-19-27R	59.2-258.6	0.0-343.0	33.8-275.1	0.0-343.0	18.5-275.1	92.3-211.4
P-19-28	59.7-271.8	0.0-343.0	33.8-275.1	0.0-343.0	18.5-296.2	73.9-238.1
P-19-30	28.2-288.3	0.0-343.0	0.0-343.0	0.0-343.0	0.0-343.0	54.1-255.1
P-19-33	--	33.8-275.1	73.9-238.1	33.8-275.1	92.3-211.4	--
P-19-35	82.8-224.5	18.5-296.2	33.8-255.1	18.5-296.2	54.1-255.1	126.4-180.6

Tab. 6 – HEDL P-19, influence of the fuel conductivity correlations on the axial extend of fuel melting, summary of the results.
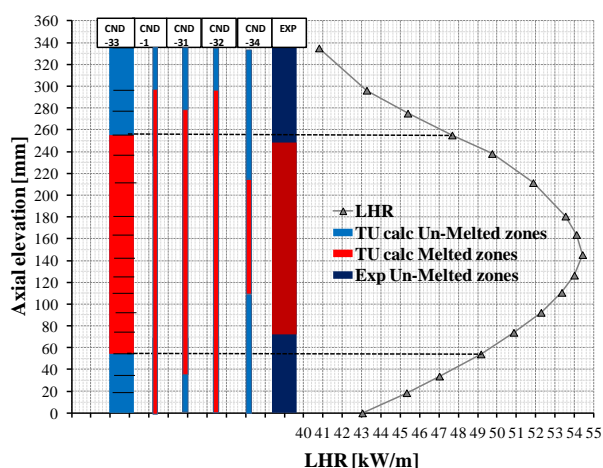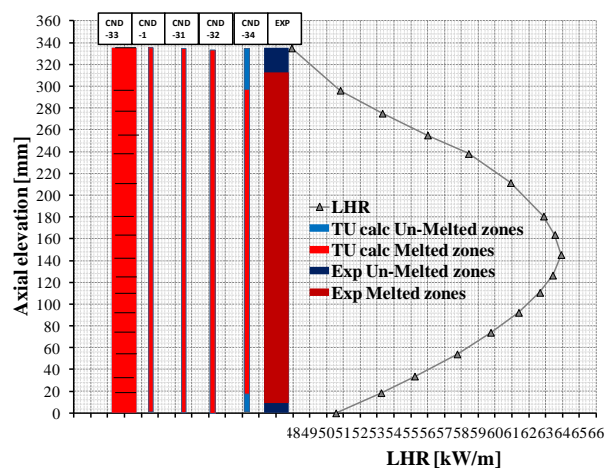
Rod P-19-2

Rod P-19-3R

Fig. 12 – HEDL P-19, influence of the relocation model on fuel melting, rods #1, 2.
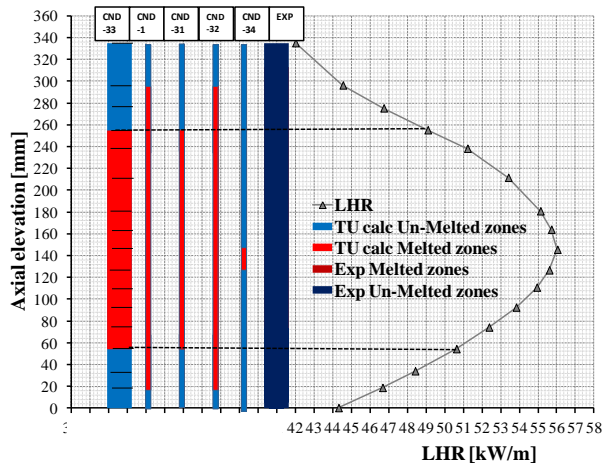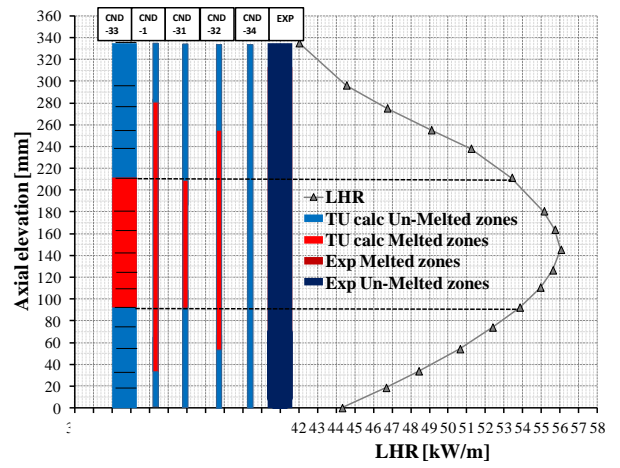
Rod P-19-5

Rod P-19-6

Fig. 13 – HEDL P-19, influence of the relocation model on fuel melting, rods #3, 4.
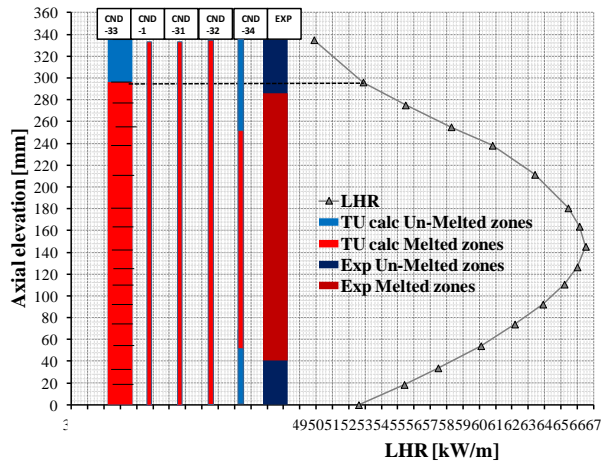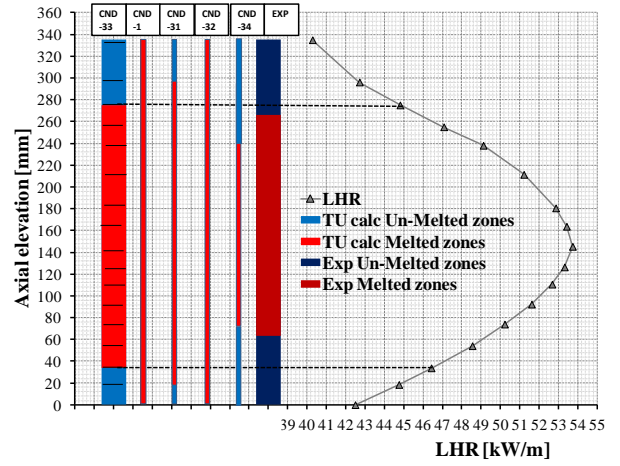
Rod P-19-7R

Rod P-19-8

Fig. 14 – HEDL P-19, influence of the relocation model on fuel melting, rods #5, 6.
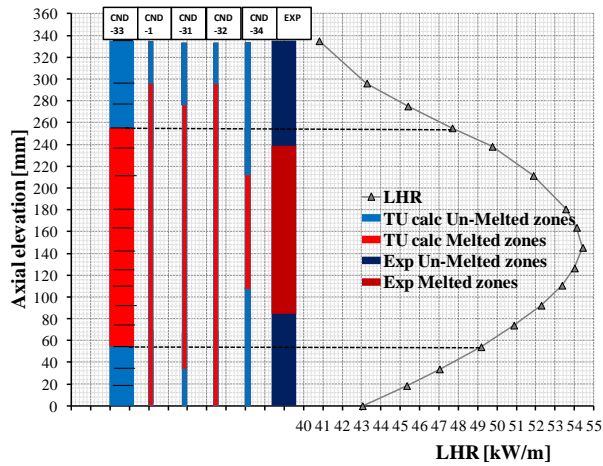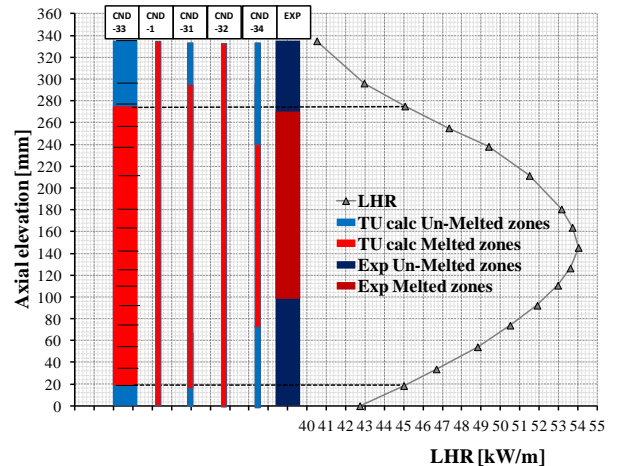
Rod P-19-13

Rod P-19-20

Fig. 15 – HEDL P-19, influence of the relocation model on fuel melting, rods #7, 8.
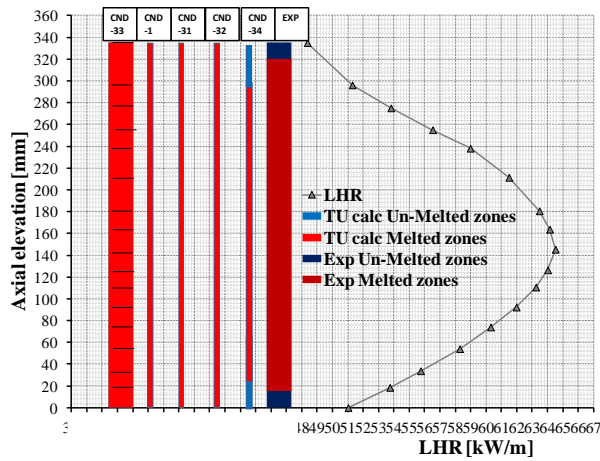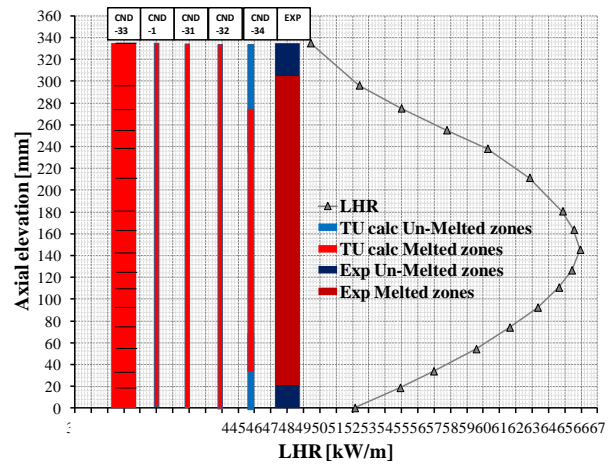
Rod P-19-24R

Rod P-19-25R

Fig. 16 – HEDL P-19, influence of the relocation model on fuel melting, rods #9, 10.
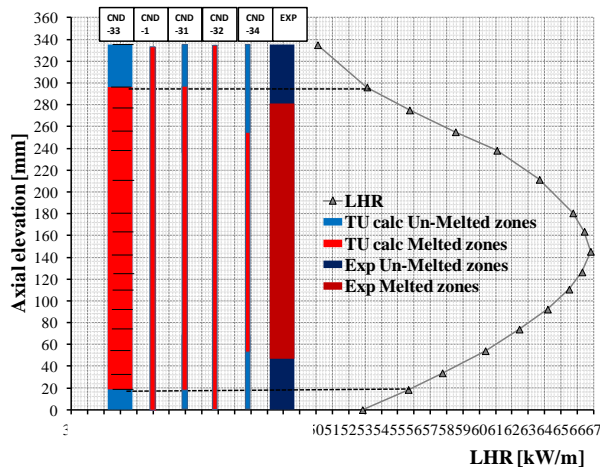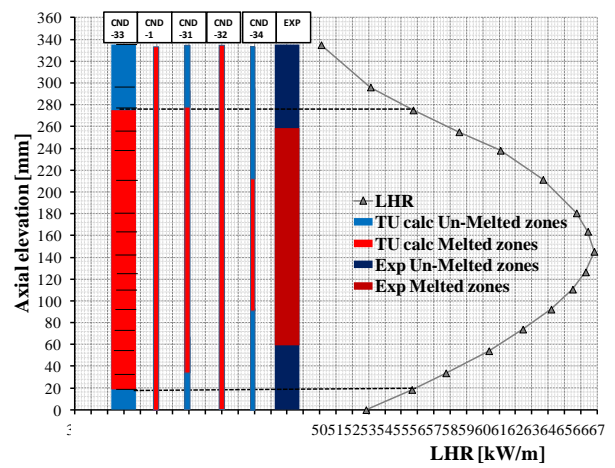
Rod P-19-26R

Rod P-19-27R

Fig. 17 – HEDL P-19, influence of the relocation model on fuel melting, rods #11, 12.
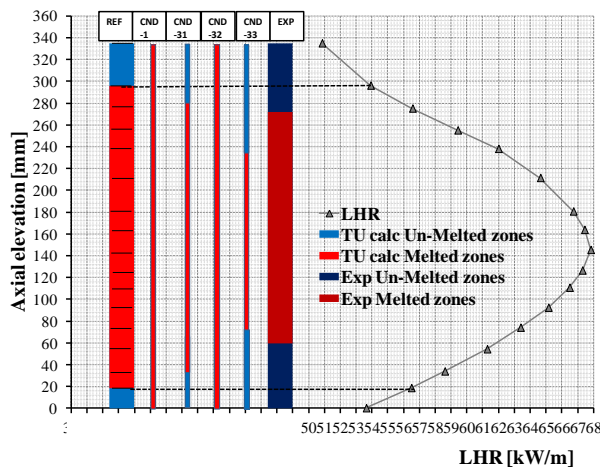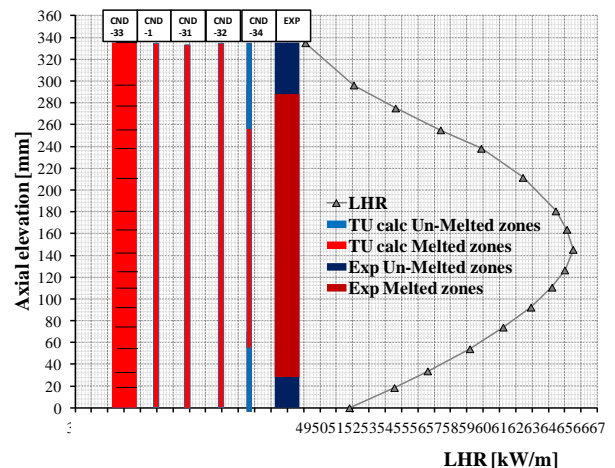
Rod P-19-28

Rod P-19-30

Fig. 18 – HEDL P-19, influence of the relocation model on fuel melting, rods #13, 14.
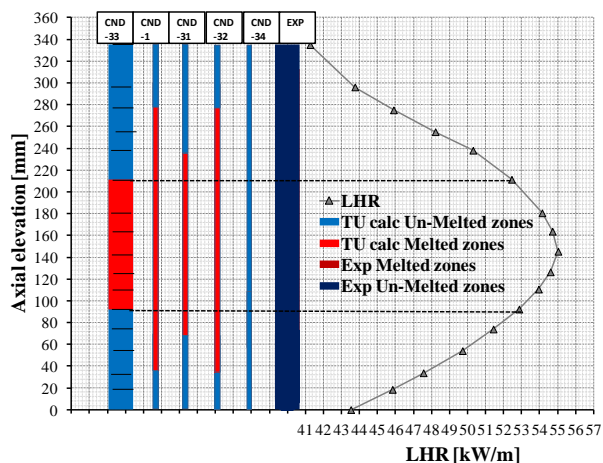
Rod P-19-33

Rod P-19-35

Fig. 19 – HEDL P-19, influence of the relocation model on fuel melting, rods #15, 16.

4 Conclusions

The capabilities of TRANSURANUS code in simulating the inception of MOX fuel melting have been assessed against HEDL P-19 experiment. It includes 16 fresh 25% PuO_2 enriched FBR rods irradiated in EBR-II to investigate the effects of initial fuel-to-cladding gap sizes, from 0.043 to 0.127 mm, on the linear-heat-rate needed to cause incipient fuel melting at beginning-of-life. The results achieved from the simulations bring to the conclusions hereafter summarized:

- The correct simulation of the gap status at the end of the experiment mainly depends on the selection of the relocation model and it is crucial to assess the fuel temperature profile. Five different options have been checked: the standard relocation (modified FRAPCON-3 model) is found to fit the experimental trend generally with minor deviations.

- The fuel conductivity correlations directly impact on the fuel temperature. Five options have been tested. Four correlations over predict the axial extension of fuel melting being therefore conservative. Among them, those of Lanning and Beyer is more close to the experiment. The correlation according to Wiesenack was developed from UO_X fuel and generally under-predicts the axial extension of fuel melting. However, it is the only one that simulates correctly the un-melted rods.

- It should be underlined that conductivity correlations have been mainly tested on LWR MOX fuel which is operated at lower temperature and contains less PuO_2 than FBR fuel. Therefore, discrepancies may be related to uncertainty of the correlations in the high temperature zone (particularly beyond 2200°C that is always exceeded in the experiment) or to the effect of high PuO_2 content (which is not directly considered in any correlation).

Future developments:

- Modeling of densification and restructuring and assessment of design tolerances such as O/M ratio, gap initial size and pellet density is not considered in this report. However, they are expected to impact on the results and deserve further investigations.

- Central void, density at pellet center and radial extension of restructuring were measured and should be therefore compared with the simulations.

- This analysis could in principle be applied to validate models and correlations for the application to overpower transient at BOL in new generation FR whose fuel is similar to those tested in HEDL-P-19 (i.e. MHYRRA, ASTRID).

REFERENCES

[1]   *Carbajo J.J., et al*. **A review of thermo-physical properties of MOX and UO₂ fuel**. Oak Ridge National Laboratory, ORNL/TM/351, 2000.

[2]   *Massih A.R.*, **Models for MOX fuel behavior, a selective review**. SKI Report 2006,10, January 2006.

[3]   *IAEA,* **Status and Advances in MOX Fuel Technology**. technical report number 415, Vienna 2003.

[4]   *Lassmann K.*, **TRANSURANUS: a fuel rod analysis code ready for use**. Journal of Nuclear Material 188 (1992) 295-302.

[5]   *Van Uffelen P.*, **Modeling of Nuclear Fuel Behavior**, **Publications Office.** JRC Publications, Report EUR 22321 EN, European Commission, 2006.

[6]   *Lassmann K., Schubert A., Van Uffelen P., Gyory Cs., van de Laar J.*, **Transuranus Handbook Version "v1m1j06"**. EC, JRC, ITU, July 2012.

[7]   *Baker R.B.*, **Integral heat rate to incipient melting in UO₂-PUO₂ FR fuel**. Hanford Engineering Development Laboratory, HEDL-TME 77-23UC-79b, 1978 U.S.

[8]   *Baker R.B.*, **Calibration of a fuel to cladding gap conductance model for fast reactor fuel pins**. Hanford Engineering Development Laboratory, HEDL-TME 77-86 UC-79, 1978 U.S.

[9]   *Ethridge J.L., et al*. **Fast Flux Test Facility Core System.** WHC-SA—0981 DE91 004559 Annerican Nuclear Society Winter Meeting Washington, D. C. November 11-15,1990.

[10]   *Miller L.B., Golden G.H., Jarka R.E., Phillips K.E.*, **Characterization of the Power in an Experimental Irradiation Subassembly of Mixed-Oxide in EBR-II**. ANL/EBR-I1-047, Argonne National Laboratory, Argonne, IL/Idaho Falls, Idaho, September 1971.

[11]   *Djurle S., et al.,* **The Super-Ramp Project**, **Final report of the Super-Ramp project**. STIR-32, Studsvik AB Atomenergi, Studsvik, Sweden ,1984.

[12]   *Rozzia D., Del Nevo A., Ardizzone A., Tarantno M., Agostini P.,* **Capabilities of TRANSURANUS Code in Simulating Inception of Melting in FBR MOX Fuel**. In Proc. of NENE-2013, paper n° 609 Bled, Slovenia, 2013 September 9-12.

[13]   *Wiesenack W.*, **Assessment of UO₂ Conductivity Degradation Based on In-pile Temperature Data**. Proceedings of the 1997 International Topical Meeting on LWR Fuel Performance, Portland, Oregon, March 2-6 (1997), p. 507.

[14]   *Rozzia D., Forgione N., Ardizzone A.,* **Analysis and Validation of FGR in MOX fuel at High Burn-ups**. ADP-PAR-2012 LP2 Task A3 deliverable LP2.a.3_b, July 2013.

[15]   *Philipponneau Y.*, **Thermal conductivity of (U, Pu) O₂₋ₓ mixed oxide fuel**. Journal of Nuclear Materials 188 (1992) 194-197.

[16]   *Schubert A., et al*., **Present Status of the MOX Version of the TU Code**. EHPG Meeting on High Burn-up Fuel Performance, Sandefjord, Norway, 9-14 May 2004

[17]   *Carbajo J.J., Yoder G.L., Popov S.G., Ivanov V.K.*, **A review of the thermo-physical properties of MOX and UO₂ fuels**. Journal of Nuclear Materials 299 (2001) 181-198

[18]   *Lanning D.D., Beyer C.E.*, **Proposed FRAPCON-3 MOX fuel thermal conductivity model compared to Halden fuel temperature data**. EHPG Meeting on High Burn-up Fuel Performance, Storefjell, Gol, Norway, 8-13 September 2002.

APPENDIX A: Comparative analyses on Relocation Models

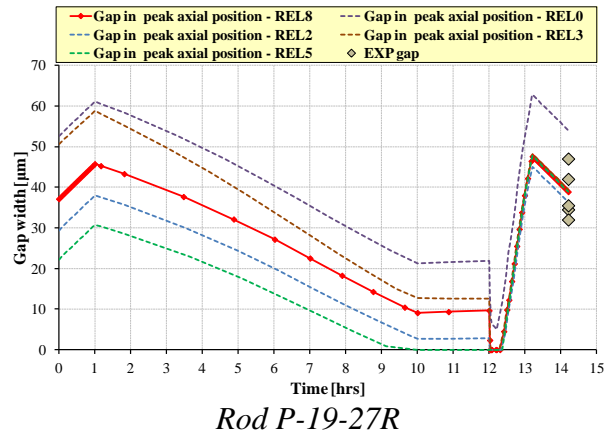## A.1 Assessment of the impact of relocation models on gap size

Rod P-19-2

Rod P-19-3R
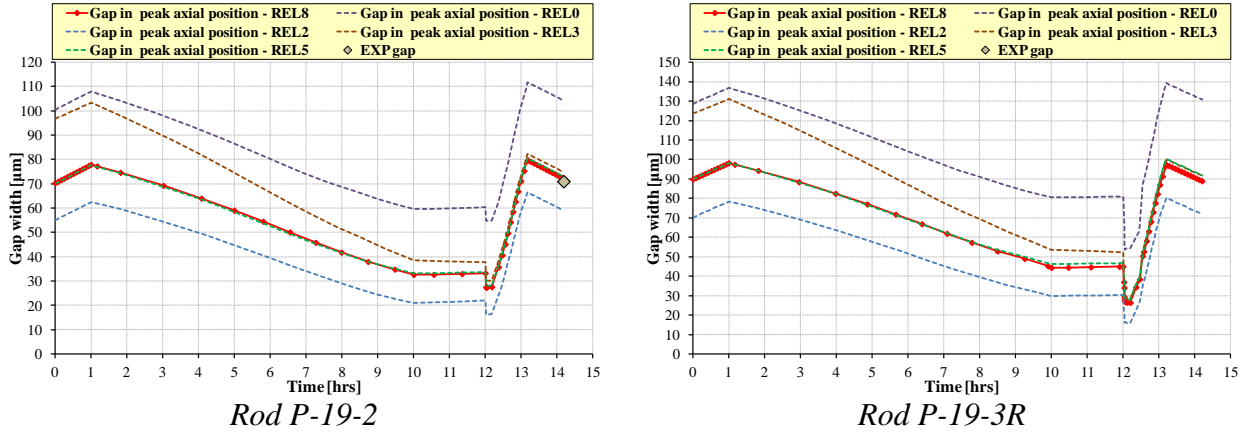
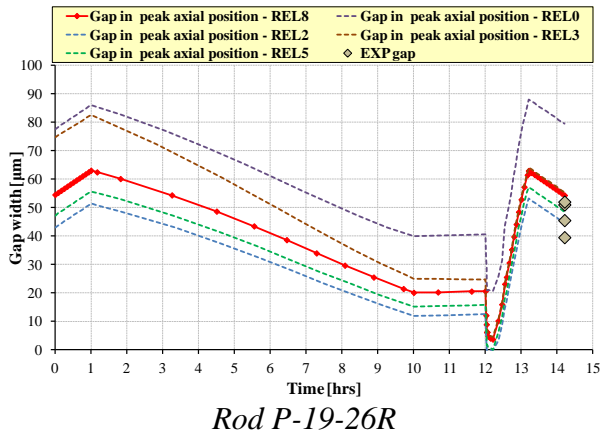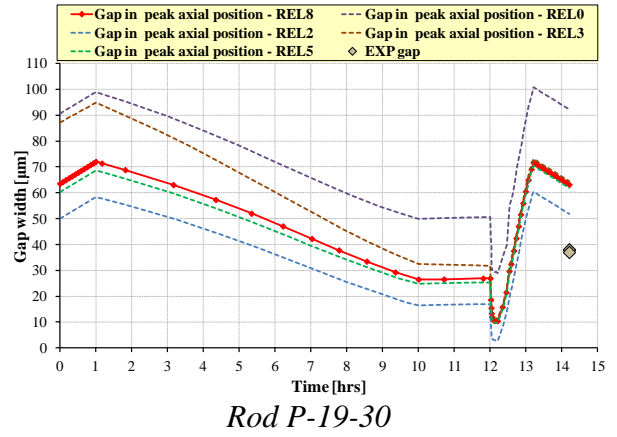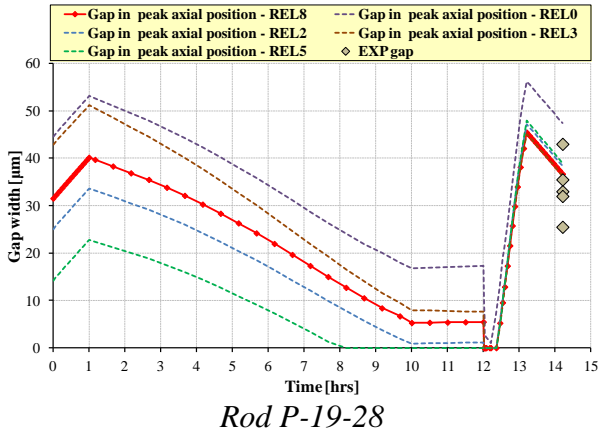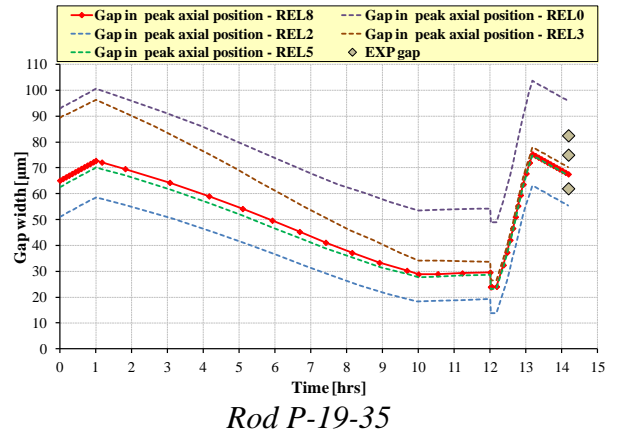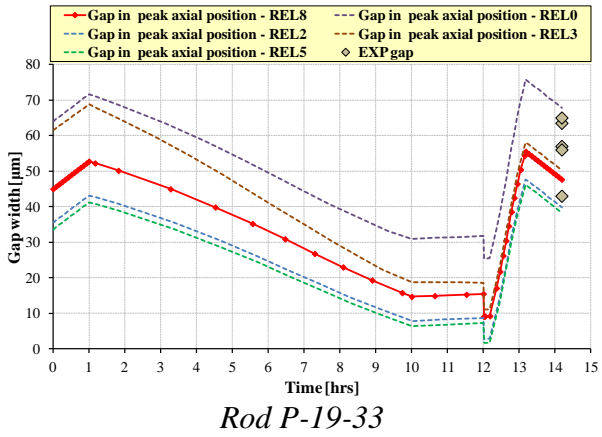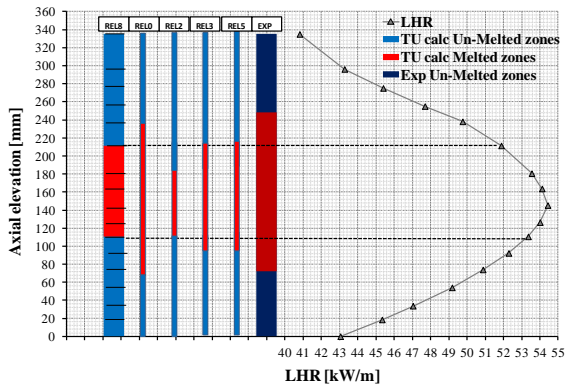*Fig. A. 1 – HEDL P-19, influence of relocation on gap trend, rods #1, 2.*

Rod P-19-5

Rod P-19-6
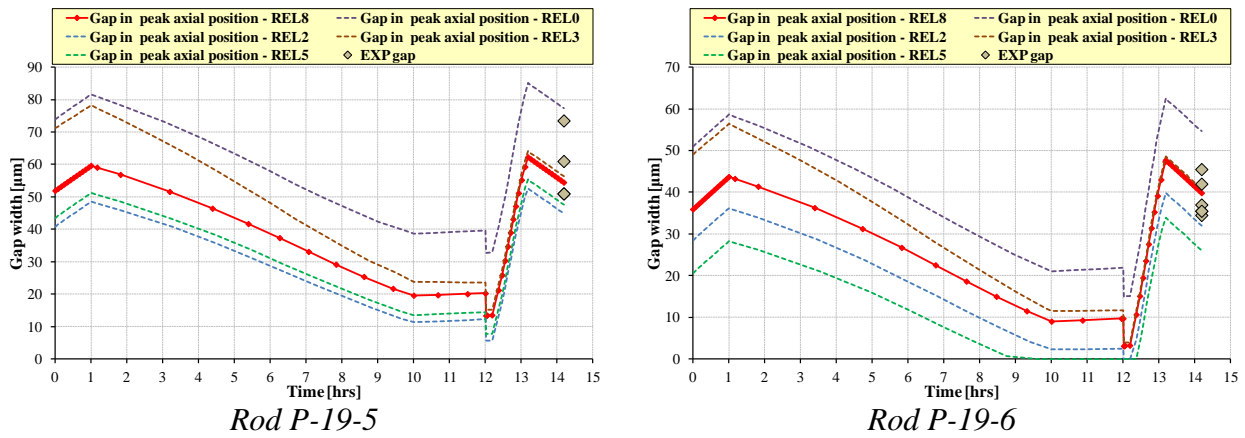
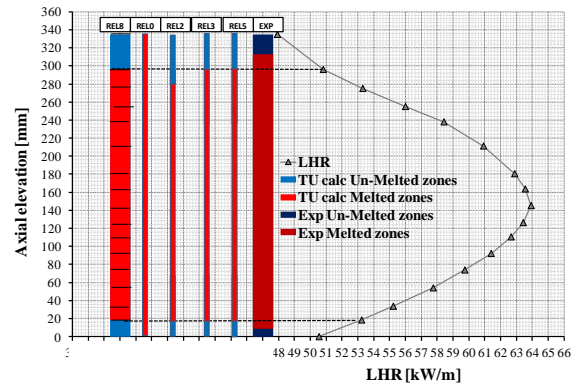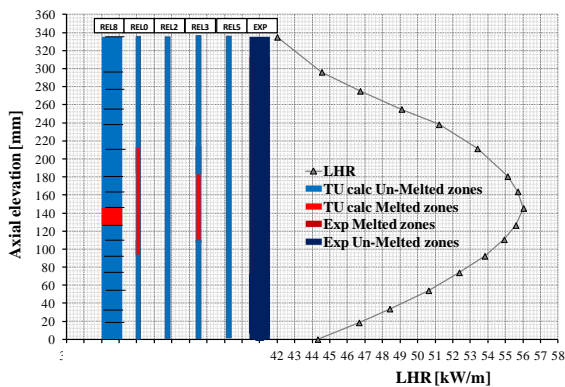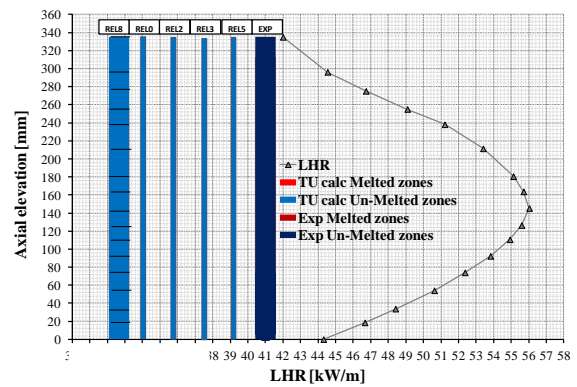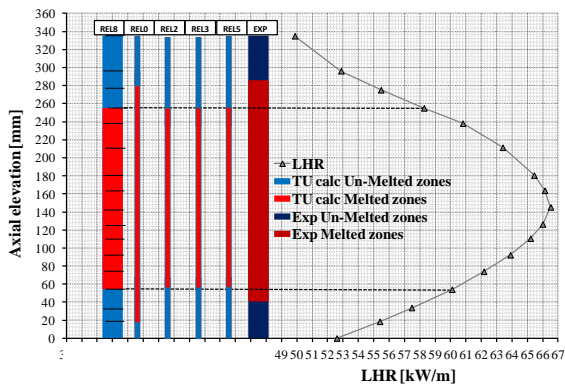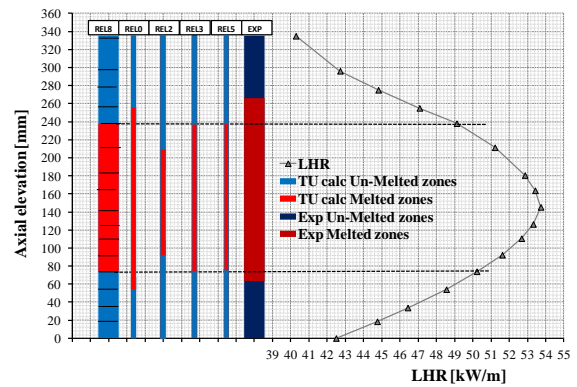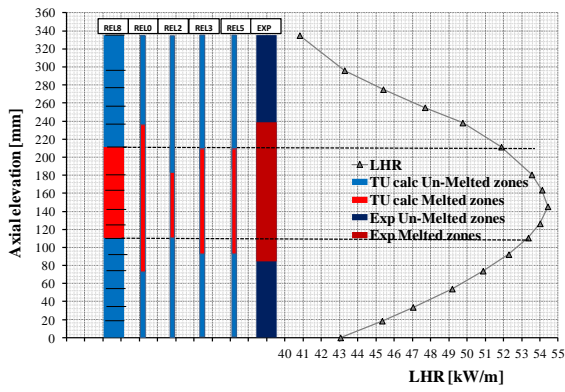*Fig. A. 2 – HEDL P-19, influence of relocation on gap trend, rods #3, 4.*

Rod P-19-7R

Rod P-19-8
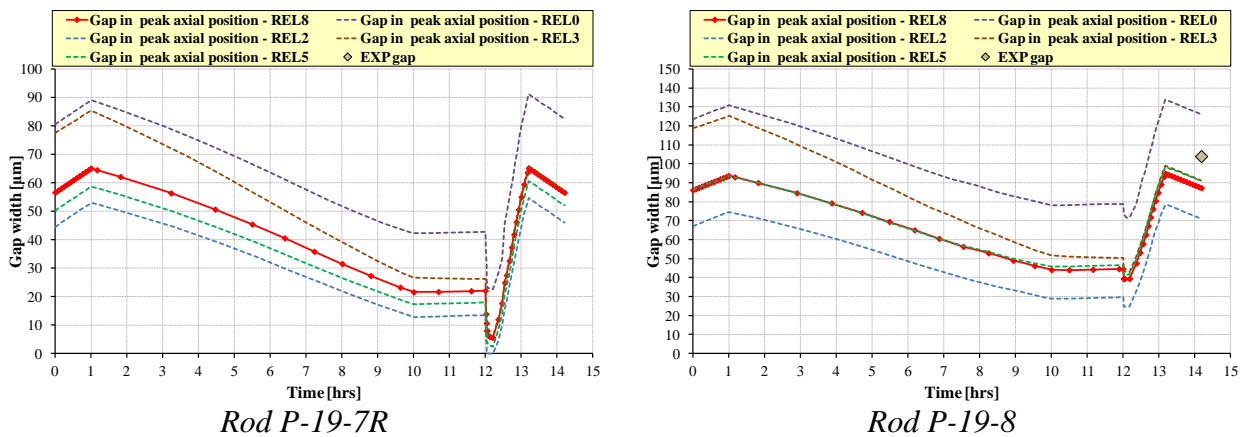
Fig. A. 3 – HEDL P-19, influence of relocation on gap trend, rods #5, 6.

Rod P-19-13   *Rod P-19-20*
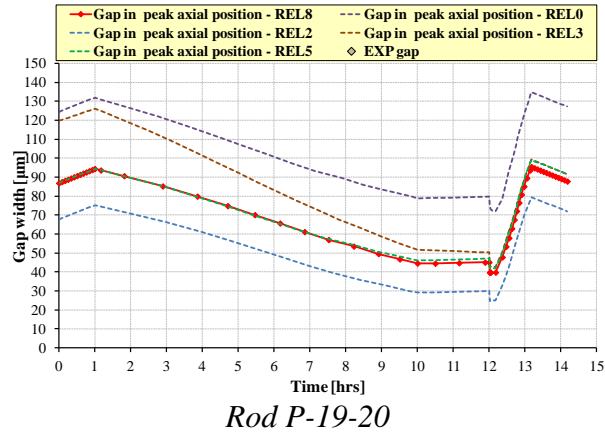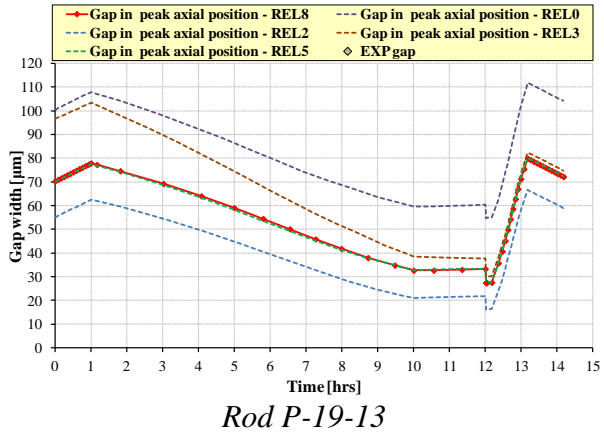
Fig. A. 4 – HEDL P-19, influence of relocation on gap trend, rods #7, 8.

Rod P-19-24R   *Rod P-19-25R*
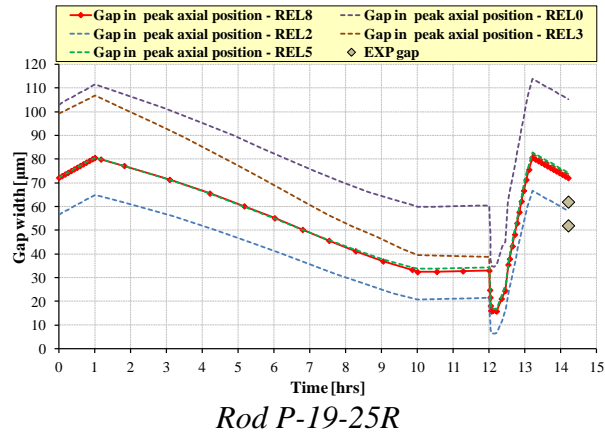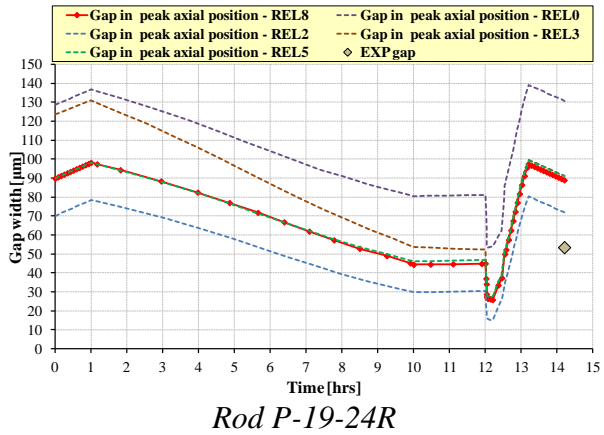
Fig. A. 5 – HEDL P-19, influence of relocation on gap trend, rods #9, 10.

Rod P-19-26R   *Rod P-19-27R*

Fig. A. 6 – HEDL P-19, influence of relocation on gap trend, rods #11, 12.

Rod P-19-28

Rod P-19-30

Fig. A. 7 – HEDL P-19, influence of relocation on gap trend, rods #13, 14.

Rod P-19-33

Rod P-19-35

Fig. A. 8 – HEDL P-19, influence of relocation on gap trend, rods #15, 16.

A.2   Assessment of the impact of relocation models on fuel melting

Rod P-19-2

Rod P-19-3R

Fig. A. 9 – HEDL P-19, influence of the relocation model on fuel melting, rods #1, 2.

Rod P-19-5

Rod P-19-6

Fig. A. 10 – HEDL P-19, influence of the relocation model on fuel melting, rods #3, 4.

Rod P-19-7R

Rod P-19-8

Fig. A. 11 – HEDL P-19, influence of the relocation model on fuel melting, rods #5, 6.
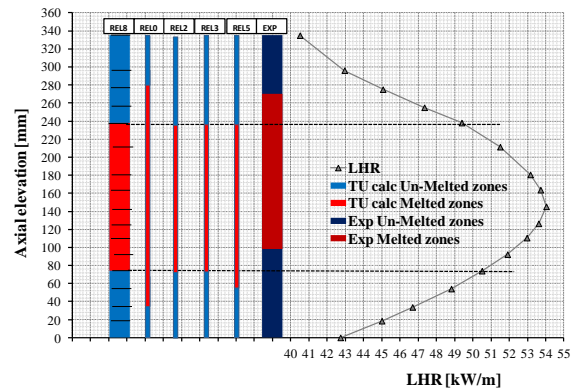
Rod P-19-13

Rod P-19-20

Fig. A. 12 – HEDL P-19, influence of the relocation model on fuel melting, rods #7, 8.
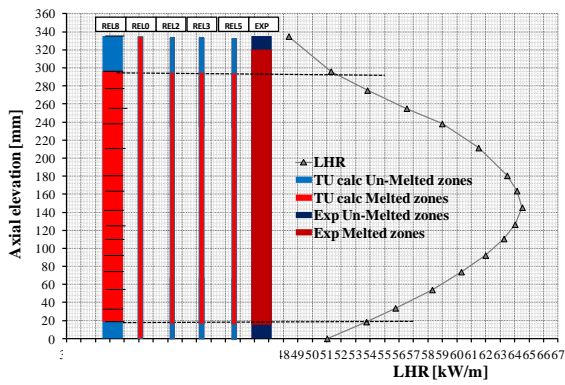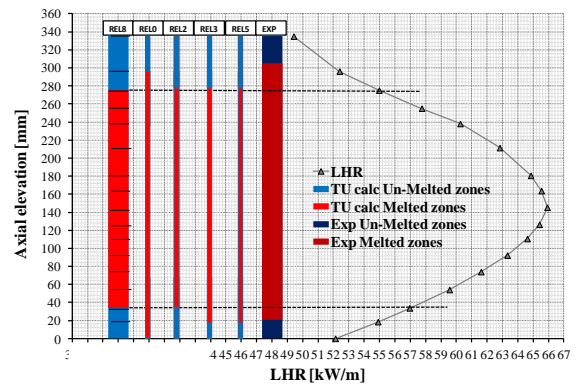
Rod P-19-24R

Rod P-19-25R

Fig. A. 13 – HEDL P-19, influence of the relocation model on fuel melting, rods #9, 10.
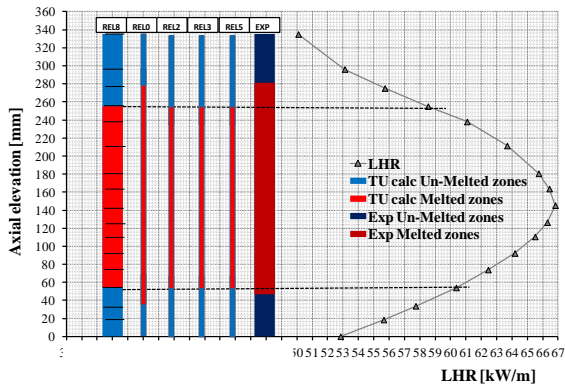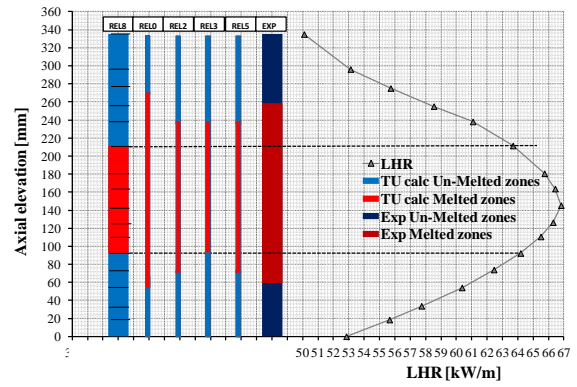
Rod P-19-26R

Rod P-19-27R

Fig. A. 14 – HEDL P-19, influence of the relocation model on fuel melting, rods #11, 12.
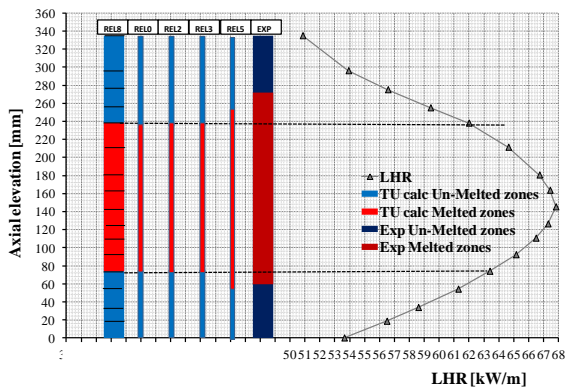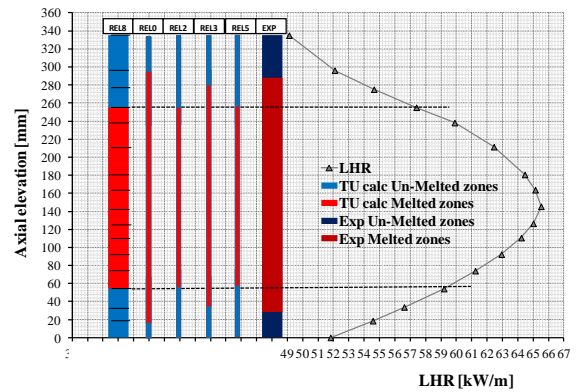
Rod P-19-28

Rod P-19-30

Fig. A. 15 – HEDL P-19, influence of the relocation model on fuel melting, rods #13, 14.
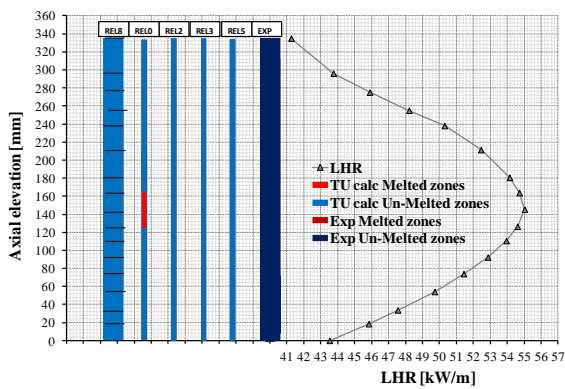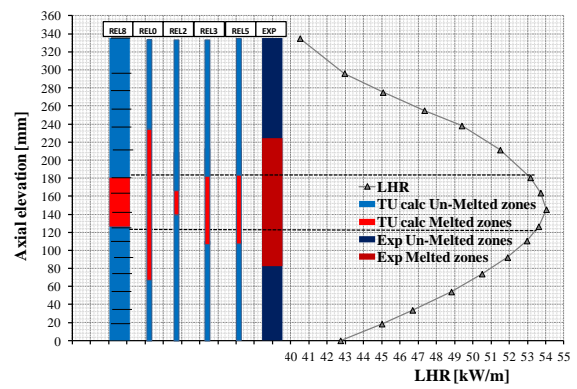
Rod P-19-33

Rod P-19-35

Fig. A. 16 – HEDL P-19, influence of the relocation model on fuel melting, rods #15, 16.

APPENDIX B: Comparative analyses on fuel conductivity

B.1 **Assessment of the impact of fuel conductivity on fuel centreline temperature**
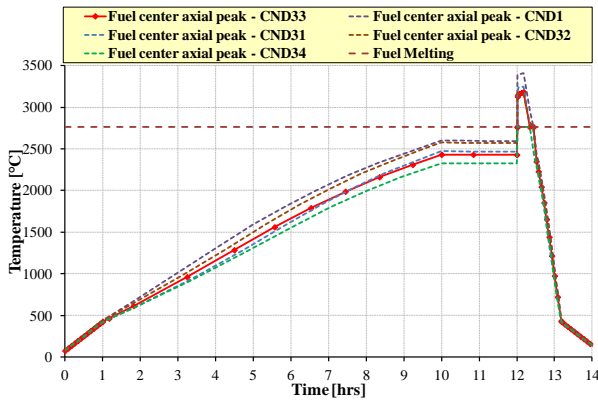
Fig. B. 1 – HEDL P-19, influence of fuel conductivity on fuel temperature in peak axial position, rod P-19-2.
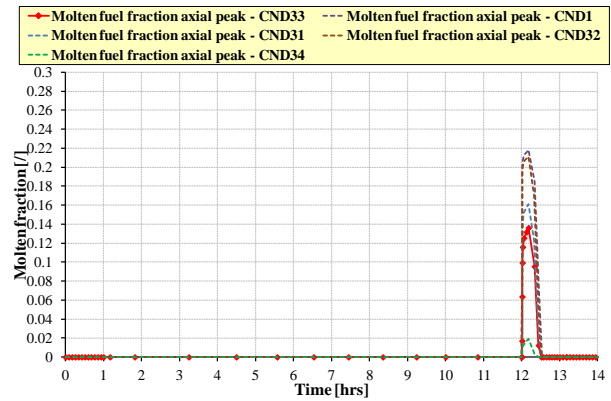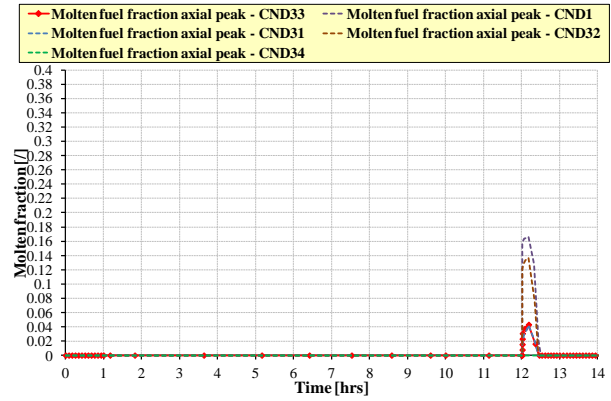

Fig. B. 2 – HEDL P-19, influence of fuel conductivity on the fuel melting fraction in peak axial section, rod P-19-2.
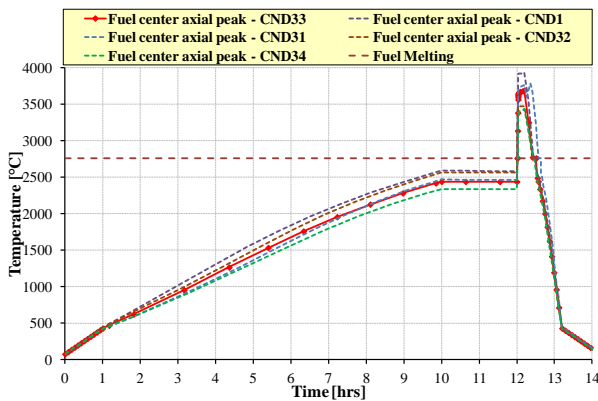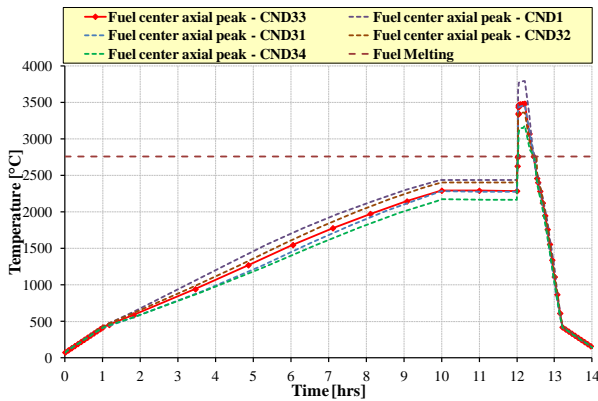

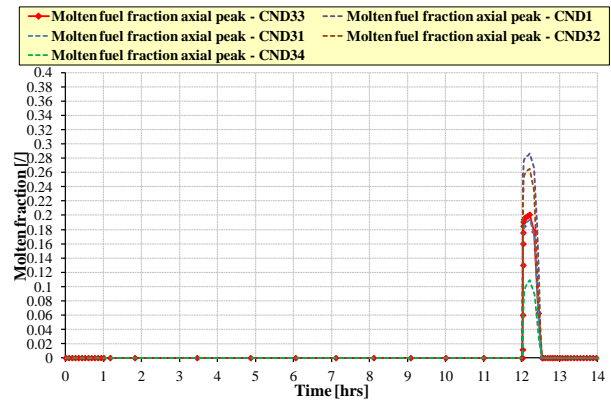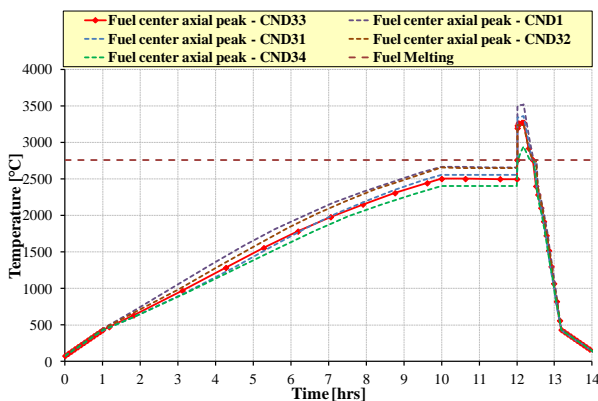*Fig. B. 3 – HEDL P-19, influence of fuel conductivity on fuel temperature in peak axial position, rod P-19-3R.*
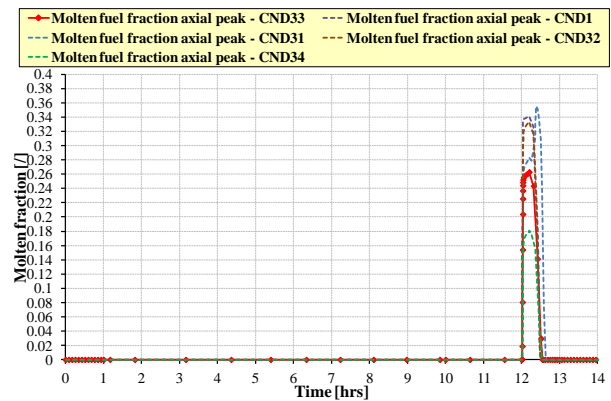
Fig. B. 4 – HEDL P-19, influence of fuel conductivity on the fuel melting fraction in peak axial section, rod P-19-3R.
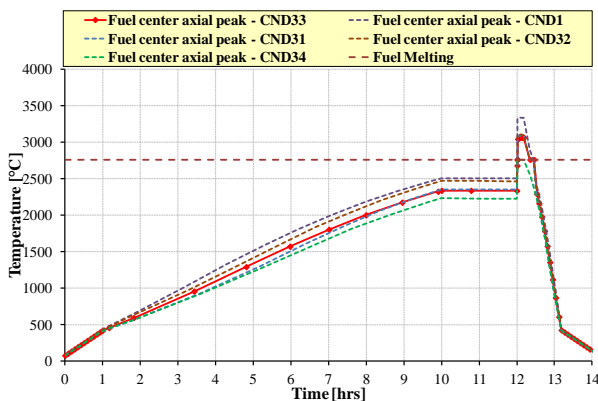
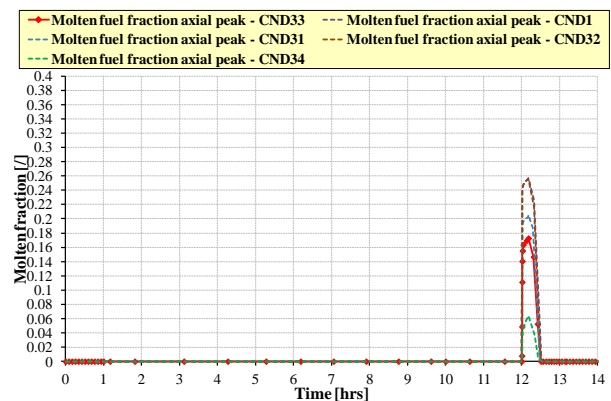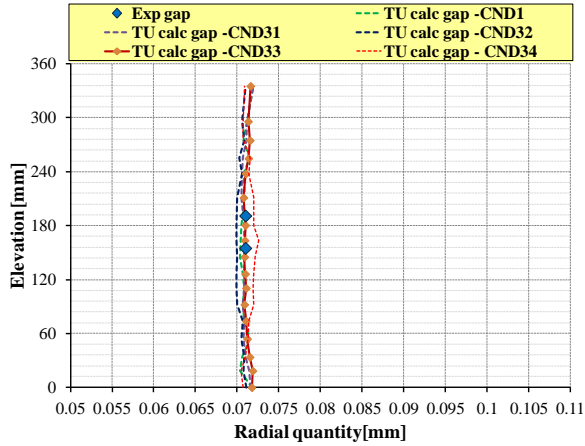*Fig. B. 5 – HEDL P-19, influence of fuel conductivity on fuel temperature in peak axial position, rod P-19-5.*
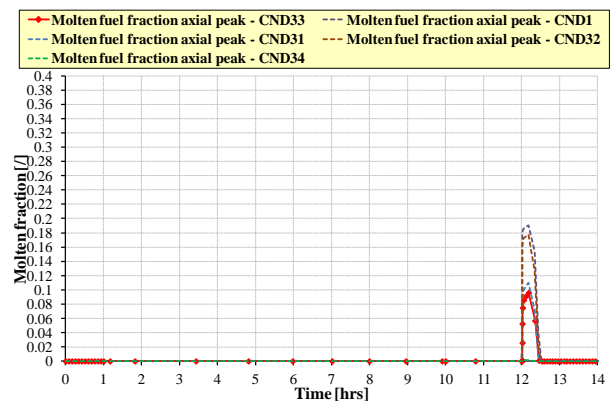
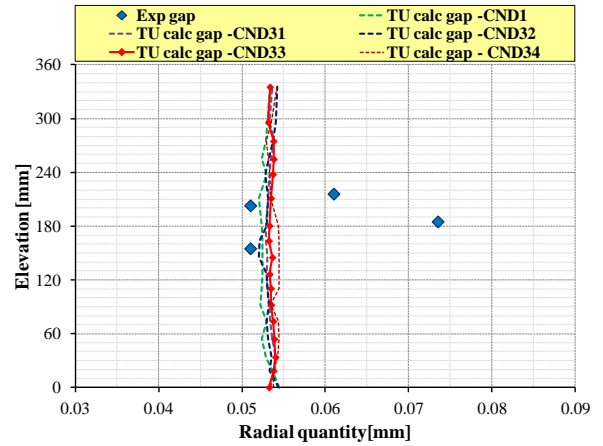*Fig. B. 6 – HEDL P-19, influence of fuel conductivity on the fuel melting fraction in peak axial section, rod P-19-5.*
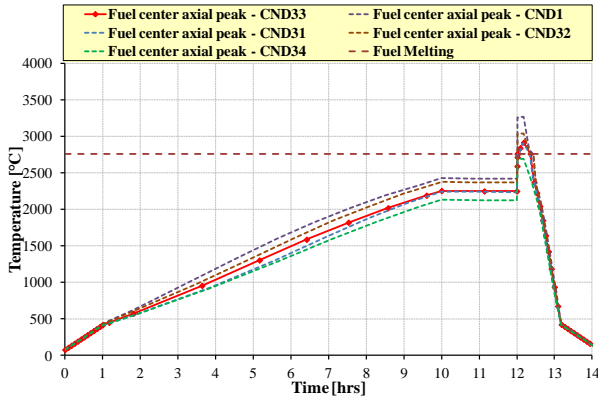
Fig. B. 7 – HEDL P-19, influence of fuel conductivity on fuel temperature in peak axial position, rod P-19-6.

Fig. B. 8 – HEDL P-19, influence of fuel conductivity on the fuel melting fraction in peak axial section, rod P-19-6.

Fig. B. 9 – HEDL P-19, influence of fuel conductivity on fuel temperature in peak axial position, rod P-19-7R.

Fig. B. 10 – HEDL P-19, influence of fuel conductivity on the fuel melting fraction in peak axial section, rod P-19-7R.

Fig. B. 11 – HEDL P-19, influence of fuel conductivity on fuel temperature in peak axial position, rod P-19-8.

Fig. B. 12 – HEDL P-19, influence of fuel conductivity on the fuel melting fraction in peak axial section, rod P-19-8.

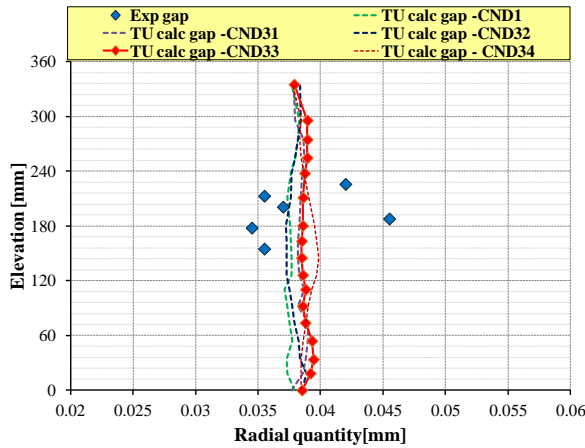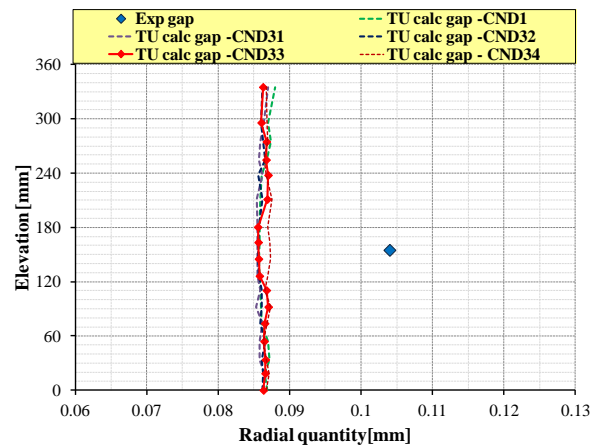## B.2 Assessment of the impact of fuel conductivity on gap size

Rod P-19-2

Rod P-19-5

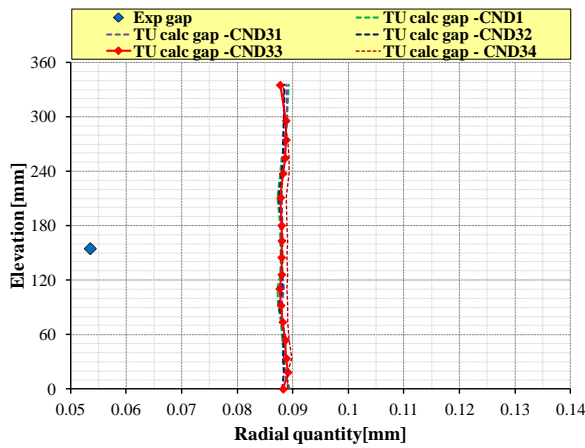*Fig. B. 13 – HEDL P-19, influence of fuel conductivity on gap size, rods #1, 3.*
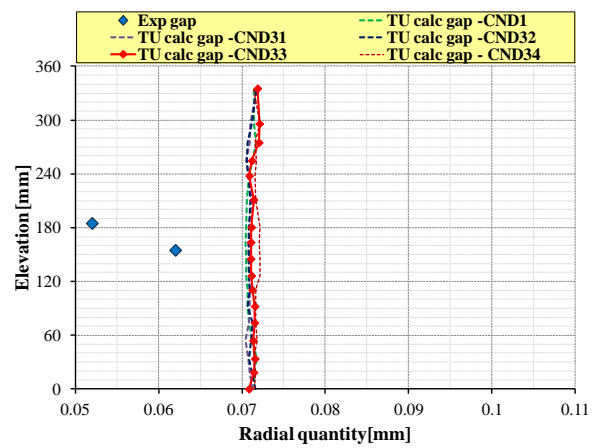

Rod P-19-6

Rod P-19-8

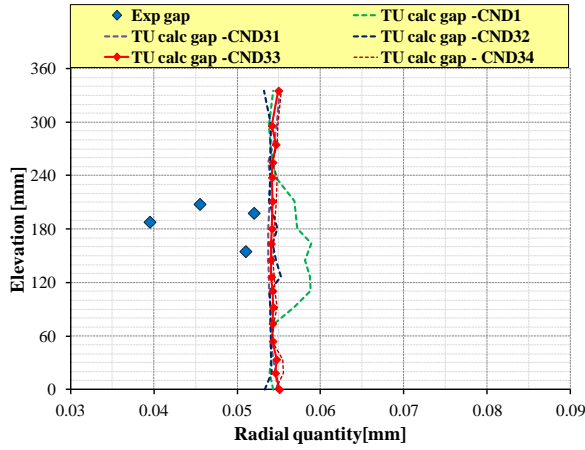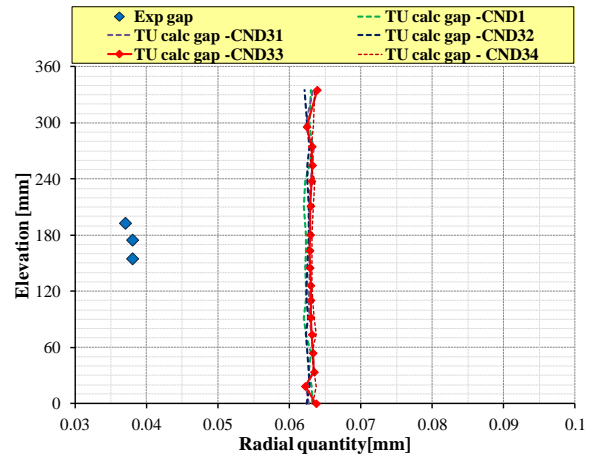*Fig. B. 14 – HEDL P-19, influence of fuel conductivity on gap size, rods #4, 6.*

Rod P-19-24R

Rod P-19-25R

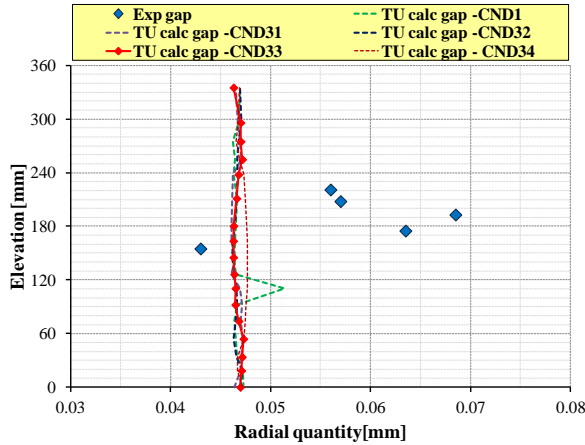*Fig. B. 15 – HEDL P-19, influence of fuel conductivity on gap size, rods #9, 10.*
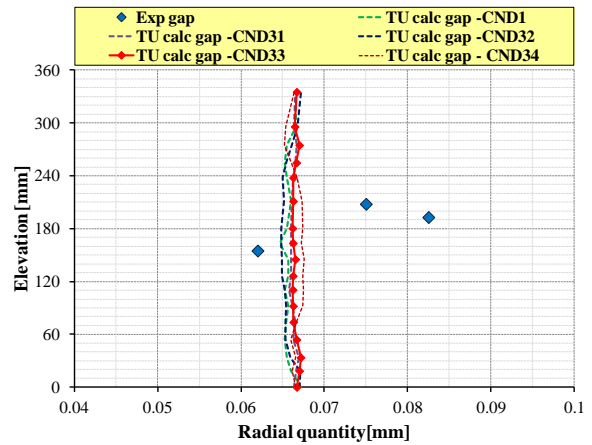
Rod P-19-26R

Rod P-19-30

Fig. B. 16 – HEDL P-19, influence of fuel conductivity on gap size, rods #11, 14.

Rod P-19-33

Rod P-19-35

Fig. B. 17 – HEDL P-19, influence of fuel conductivity on gap size, rods #15, 16.